Politecnico di Torino

Corso di Laurea Magistrale in Ingegneria Chimica e dei Processi Sostenibili
A.a. 2024/2025
Sessione di Laurea Ottobre 2025

Electrochemical Reduction of CO_2 to Acetate

The role of copper-based catalysts

Relatori:
prof. Stefania Specchia
prof. Plamen Atanassov

Candidato:
Antonio Galuppo

Contents

Index for images

Index for tables

Prefazione

La seguente tesi sperimentale è stata realizzata negli Stati Uniti presso la University of California Irvine (UCI), sotto la supervisione della Prof. Stefania Specchia e del Prof. Plamen Atanassov e del suo gruppo di ricerca. Il lavoro ha riguardato la sintesi, la caratterizzazione e la valutazione dell'attività nei confronti della riduzione elettrochimica dell'anidride carbonica (CO2RR) di diversi catalizzatori a base di rame.

In particolare, sono stati sintetizzati 3 nuovi catalizzatori, di cui 2 a base di rame ed uno contenente nanoparticelle di argento, attraverso un metodo di sintesi già precedentemente utilizzato dal gruppo di ricerca per la sintesi di catalizzatori contenenti platino e cobalto, adattandolo ai composti chimici di interesse.

Successivamente alla sintesi, l'attività di ricerca ha posto l'attenzione sulla caratterizzazione degli stessi, utilizzando come metodologia la Diffrazione a Raggi X (XRD) e la Microscopia Elettronica a Trasmissione (TEM), per verificare le fasi cristalline presente e la morfologia e la dimensione dei cristalli ottenuti.

Infine, sono state testate le prestazioni di tali catalizzatori nei confronti della riduzione elettrochimica della CO_2, utilizzando come configurazione sperimentale le flow cell, degli elettrolizzatori contenenti un elettrodo a diffusione gassosa (GDE), che ci consente di ridurre i problemi dovuti al trasporto di massa del gas utilizzato.

Parallelamente, è stato analizzato anche l'effetto del pH sulla distribuzione dei prodotti liquidi ottenuti dalla riduzione del monossido di carbonio, utilizzando come catalizzatore delle particelle commerciali di rame, sempre in un elettrolizzatore a flusso.

I prodotti ottenuti da questi esperimenti sono stati poi quantificati utilizzando la cromatografia liquida ad alte prestazioni, da cui è possibile analizzare l'andamento rispetto al pH e rispetto al voltaggio di cella utilizzato.

La tesi è stata suddivisa nei seguenti capitoli:

- Capitolo 1: Introduzione generale sulla sostenibilità e sullo stato dell'arte attuale della CO2RR, soffermandosi sulle basi teoriche della stessa e sui diversi sistemi utilizzati;

- Capitolo 2: Vengono elencati i materiali utilizzati e vengono descritte le metodologie di sintesi e di caratterizzazione dei nuovi catalizzatori così come i macchinari utilizzati per la quantificazione dei prodotti. Vengono inoltre riassunti tutti i principali test effettuati;

- Capitolo 3: Si riportano i risultati ottenuti con relativa discussione, attraverso l'ottenimento di grafici;

- Capitolo 4: Conclusioni e prospettive future.

I. Introduzione

I.I Cambiamenti climatici ed emissioni di CO_2

Il cambiamento climatico è una delle sfide più complesse del nostro tempo, con risvolti ambientali, economici e sociali. Una delle cause principali è l'aumento continuo delle concentrazioni di anidride carbonica (CO_2) in atmosfera, dovuto soprattutto a combustibili fossili, deforestazione e processi industriali [1,2].

Negli ultimi decenni le emissioni antropiche di CO_2 hanno superato i 30 miliardi di tonnellate all'anno. Dopo una leggera riduzione durante la pandemia da COVID-19, la tendenza alla crescita è ripresa, come mostrato in Fig. 1. Questo aumento ha già portato la temperatura media globale a un incremento di oltre 1.1 °C rispetto all'epoca preindustriale, con conseguenze potenzialmente irreversibili che potrebbero durare secoli [3].

Le proiezioni mostrano che senza interventi rapidi e incisivi, entro fine secolo l'aumento della temperatura potrebbe superare i 2 °C, ben oltre il limite fissato dall'Accordo di Parigi del 2015, con rischi gravi per gli equilibri climatici globali [4].

Gli effetti sono già visibili: innalzamento del livello dei mari, eventi meteorologici estremi sempre più frequenti e danni agli ecosistemi [5]. Affrontare la crisi climatica richiede di ridurre drasticamente le emissioni, spostandosi dai combustibili fossili verso le energie rinnovabili [6].

Tra le strategie proposte, il carbon capture and storage (CCS) riduce le emissioni immagazzinando la CO_2 nel sottosuolo. Tuttavia, questo approccio ha lo svantaggio di non creare valore economico. Al contrario, il carbon capture and utilization (CCU) mira a trasformare la CO_2 in prodotti utili come carburanti, polimeri e intermedi chimici, coniugando vantaggi ambientali e opportunità di mercato [7].

I.II Riduzione elettrochimica della CO_2

La riduzione elettrochimica della CO_2 (CO_2RR) è una delle tecnologie più promettenti per affrontare la crisi climatica. Si basa sulla conversione della CO_2 in prodotti a valore aggiunto utilizzando energia elettrica, che può provenire da fonti rinnovabili come solare ed eolico. In questo modo, la CO_2RR non solo chiude il ciclo del carbonio, ma può diventare un processo a bilancio negativo di emissioni [8].

Dal punto di vista termodinamico, però, la CO_2 è una molecola molto stabile e poco reattiva. I suoi doppi legami C=O sono molto forti e per romperli servono catalizzatori o un apporto

energetico significativo [9]. Inoltre, in soluzioni acquose la reazione compete direttamente con l'evoluzione dell'idrogeno (HER), che abbassa l'efficienza faradica.

Nonostante questi limiti, la via elettrochimica offre vantaggi unici: controllo preciso dei parametri di reazione (potenziale, densità di corrente, pH), modularità degli impianti, possibilità di accoppiamento diretto con fonti rinnovabili e produzione decentralizzata [10].

Un elettrolizzatore tipico è composto da un catodo, dove avviene la riduzione della CO_2, un anodo, dove tipicamente si ha l'ossidazione dell'acqua tramite la reazione di evoluzione dell'ossigeno (OER) e un elettrolita. La configurazione della cella, come H-Cell, Flow Cell o altre configurazioni, inoltre, influisce molto su efficienza, stabilità e scalabilità.

Tra tutti i fattori, però, il catalizzatore è quello più cruciale: deve attivare la CO_2, stabilizzare gli intermedi e orientare la reazione verso i prodotti desiderati. In questo campo, il rame (Cu) è particolarmente interessante perché è l'unico metallo in grado di favorire la formazione di prodotti multicarboniosi (C_2^+), come acido acetico ed etanolo [11]; per questo i catalizzatori a base di rame sono molto interessanti per applicazioni chimiche ed energetiche.

I.III Aspetti termodinamici

La CO_2 è una molecola lineare, molto stabile grazie ai suoi forti doppi legami C=O, con un'entalpia di legame di circa 750 kJ/mol, il che la rende poco reattiva. La riduzione elettrochimica richiede quindi un sovrapotenziale, ossia una tensione extra rispetto a quella teorica, per superare le barriere cinetiche e favorire la formazione di intermedi [12,13].

La Tab. 1 riporta i potenziali standard delle principali reazioni di riduzione della CO_2 [14].

Prodotti semplici come monossido di carbonio (CO) e acido formico hanno valori più favorevoli, mentre quelli multicarboniosi (etanolo, propanolo, acido acetico) richiedono processi più complessi e multi-elettronici.

In condizioni reali, i sovrapotenziali necessari sono molto più alti di quelli teorici. Ad esempio, per il CO la riduzione teorica avviene a –0,11 V, ma in pratica servono valori tra –0,5 e –1,0 V. Questo divario dipende da fattori come cinetiche lente, adsorbimento degli intermedi e accoppiamento protoni-elettroni.

I.IV Il ruolo del rame

I catalizzatori per CO_2RR si dividono in quattro grandi gruppi:

- Ag e Au: selettivi verso CO.
- Pb, Hg, In: selettivi verso formiato.
- Pt, Fe: quasi inattivi, favoriscono la formazione di idrogeno.

- Cu: unico metallo capace di produrre un'ampia gamma di idrocarburi e ossigenati [14].

Il rame ha un legame intermedio con *CO: abbastanza forte da trattenerlo e trasformarlo, ma non così forte da disattivare il catalizzatore [16]. Questo equilibrio lo rende capace di stabilizzare intermedi chiave (*CO, *CHO, *OCCO) e di promuovere la formazione di legami C–C [17].

Cu è quindi essenziale per ottenere molecole C_2^+, più dense di energia e più interessanti commercialmente, ma presenta limiti: bassa selettività, produce cioè molti sottoprodotti, richiesta di alti sovrapotenziali e stabilità non ottimale [18,19].

Per superare questi problemi, si stanno sviluppando strategie come nanostrutturazione, ossidi derivati, leghe e modifiche superficiali, per mirare a migliorare la selettività, ridurre i sovrapotenziali e stabilizzare l'attività catalitica nel tempo.

I.V Meccanismi di riduzione

I.V.I Prodotti C_1

Monossido di carbonio: il meccanismo verso CO prevede la formazione di un intermedio adsorbito sulla superficie *COOH. Dopo l'adsorbimento della CO_2, si hanno delle reazioni di trasferimento accoppiato protone-elettrone (PCET) con la formazione di *COOH, che è poi ridotto a *CO, come mostrato in Fig. 3.

Formiato: il meccanismo verso il formiato prevede invece la formazione dell'intermedio *OCHO, che viene rilasciato poi come $HCOO^-$ (Fig. 4).
Questi due percorsi sono spesso alternativi e servono anche come precursori per prodotti più complessi.

I.V.II Etanolo e 1-Propanolo

Etanolo: deriva da dimerizzazione di *CO → *OCCO, si hanno poi delle reazioni PCET che portano alla formazione di diversi intermedi, fino alla liberazione dell'etanolo, come mostrato in Fig. 5.

1-Propanolo: richiede un accoppiamento extra, *CO + $*CH_2CHO$, molto più difficile, e per questo si ottiene con basse efficienze faradiche (Fig. 6) [22].

I.V.III Acetato

Il meccanismo che porta alla formazione di acetato non è ancora chiarito del tutto. Una via proposta coinvolge una prima reazione di *CO con uno ione idrossido adsorbito (*OH), invece che la dimerizzazione del monossido di carbonio, portando alla formazione di *COOH. Successivamente si ha un altro accoppiamento carbonio-carbonio che produce *COCOOH. Infine, si hanno degli step PCET che formano infine acetato, come si evince dalla Fig. 7 [23].

Questo percorso richiede alta copertura di *CO e disponibilità di *OH, favorita ad alti pH. Tuttavia, con CO_2 ciò è difficile perché a pH elevato la CO_2 si trasforma in carbonati e bicarbonati inattivi. Con CO come reagente, invece, il processo è molto più agevole e si può operare ad esempio utilizzando una soluzione 1M di KOH come elettrolita.
Basandoci su questa osservazione, abbiamo cercato di produrre un nuovo catalizzatore capace di trattenere ioni idrossido vicino la propria superficie, in modo da incrementare il pH locale, favorendo quindi la produzione di acetato.

I.VI Elettrolizzatori

I.VI. I H-Cell

È un sistema semplice, economico e utile per studi fondamentali grazie alla sua versatilità. Essa consiste di due camere riempite con un liquido separate da una membrana a scambio ionico, dando una forma ad H. Essa permette di analizzare gas e liquidi separatamente, ma soffre di limiti di trasporto di massa, con basse densità di corrente e poca produttività [24]; a cause di questo è necessario condurre gli esperimenti per un lungo periodo di tempo, in modo tale da poter raggiungere il limite di rilevamento.

I.VI.II Flow Cell

Negli ultimi anni, le celle a flusso sono emerse come un'alternativa più avanzata rispetto alle tradizionali celle di tipo H per la riduzione elettrochimica della CO_2, soprattutto quando si punta a raggiungere densità di corrente e produttività di interesse industriale.

La caratteristica distintiva di una cella a flusso è il suo funzionamento continuo: CO_2 gassosa ed elettrolita liquido vengono alimentati costantemente all'interno del sistema, consentendo una maggiore produttività e un trasporto di massa più efficiente.

In genere, una cella a flusso è costituita da un elettrodo a diffusione gassosa (GDE) al catodo, un elettrolita liquido in flusso, un comparto anodico separato da una membrana a scambio ionico.

Un GDE è tipicamente formato da uno strato di supporto poroso e idrofobico, che permette al gas CO_2 di diffondere attraverso di esso, e da uno strato catalitico sul lato frontale, a contatto con l'elettrolita liquido. Questo design crea la cosiddetta interfaccia a tre fasi (gas, liquido e solido/catalizzatore), condizione essenziale per reazioni elettrochimiche rapide ed efficienti.

Uno schema della cella a flusso è riportato in Fig. 9.

Questa configurazione consente la fornitura diretta di CO_2 gassosa alla superficie catalitica, superando in modo significativo i limiti di trasporto di massa legati alla bassa solubilità della CO_2 nei mezzi acquosi [25]. Grazie a questo, le celle a flusso possono sostenere densità di

corrente molto più elevate, spesso superiori a 200 mA cm^{-2}, mantenendo comunque una buona selettività verso i prodotti desiderati. Inoltre, la natura continua del sistema permette un migliore controllo delle interfacce gas–liquido–solido, una riduzione dello spessore dello strato di diffusione e un incremento delle efficienze faradiche. Tutto ciò rende le celle a flusso una piattaforma più pratica per lo scale-up della riduzione elettrochimica della CO_2, specialmente se integrate con fonti di energia rinnovabile [27].

Tuttavia, i vantaggi delle celle a flusso comportano anche dei compromessi. Il loro design e funzionamento risultano più complessi rispetto alle H-Cell, richiedendo un controllo preciso dei flussi di gas e liquido, oltre a un'attenta gestione di fenomeni di allagamento o disseccamento negli elettrodi a diffusione gassosa. Un'altra sfida aperta riguarda la stabilità a lungo termine: la degradazione del catalizzatore, il crossover dell'elettrolita e il fouling della membrana possono limitare il funzionamento continuo. Inoltre, se da un lato gli strati a diffusione gassosa facilitano l'accesso della CO_2, dall'altro rendono più complesso mantenere le interfacce a tre fasi in cui CO_2, elettrolita e catalizzatore interagiscono in modo efficace.

Nonostante queste difficoltà, le celle a flusso sono attualmente considerate l'architettura più promettente per colmare il divario tra la ricerca su scala di laboratorio e le applicazioni reali. Il loro design modulare le rende compatibili con sistemi reattoristici impilabili, e i progressi continui nei materiali delle membrane, nella progettazione degli elettrodi e nell'ottimizzazione degli elettroliti stanno spingendo sempre più in là le prestazioni della CO_2RR in celle a flusso [28].

I.VII Mercato e applicazioni dei prodotti CO_2RR

- Acido formico: usato in chimica industriale e come vettore di idrogeno. Mercato in crescita da 2,3 a 3,8 miliardi $ (2024–2034) [29,30].
- Acido acetico: fondamentale per VAM, alimenti e farmaceutica. Valore previsto: da 13,8 a 23 miliardi $ (2023–2030) [31].
- Etanolo: carburante, solvente e chimico di largo consumo. Mercato oltre 90 miliardi $ nel 2023 [32,33].
- 1-Propanolo: usato come solvente e intermedio. Mercato più piccolo (≈215 milioni $ nel 2023), ma di grande interesse per il valore scientifico [34].

I.VIII Obiettivi

L'obiettivo principale di questa tesi è comprendere più a fondo il comportamento catalitico del rame nella riduzione elettrochimica di anidride carbonica e monossido di carbonio. Particolare attenzione è rivolta al ruolo dell'elettrolita, e in particolare all'effetto del pH, nella modulazione dell'attività e della stabilità degli intermedi chiave durante i processi di riduzione di CO_2 e CO.

Oltre a indagare i meccanismi catalitici di base, la tesi si propone anche di esplorare la sintesi di un nuovo catalizzatore a base di rame, progettato per aumentare la selettività verso l'acido acetico, un prezioso prodotto multi-carbonioso.

Combinando attività sperimentali con i più recenti contributi presenti in letteratura, lo scopo è quello di favorire lo sviluppo di sistemi catalitici più efficienti e selettivi, capaci di valorizzare la CO_2 nell'ambito delle tecnologie energetiche del futuro.

II. Setup sperimentale

II.I Reagenti

Nitrato di rame (II) emipentaidrato (purezza ≥ 98%), nanoparticelle di rame (dimensione TEM = 25 nm), nanoparticelle di argento (dimensione TEM ≤ 100 nm), bicarbonato di potassio (purezza ≥ 99,7%), ossido di deuterio (D_2O, 99,8% atomi D), dimetilsolfossido-d6 (DMSO) e soluzione di resina perfluorurata Nafion al 5% in peso sono stati acquistati da Sigma-Aldrich (USA). Idrossido di potassio (purezza ≥ 85,0%) da MG Scientific (USA). Isopropanolo (IPA, purezza ≥ 99,9%), acetone (purezza ≥ 99,5%) e acido cloridrico (36,5–38% in peso) da Fisher Chemical (USA). Idrossido di ammonio (28–30% in peso) da VWR (USA). FCX650SE da Cabot (USA). CO (purezza ≥ 99%) da Praxair (USA). CO_2 (purezza ≥ 99,5%) e H_2/Ar (5% H_2, 95% Ar) da AirGas (USA). L'acqua ultrapura deionizzata è stata ottenuta con un sistema Millipore Milli-Q (conducibilità a 25 °C = 0,056 $\mu S \cdot cm^{-1}$).

II.II Un nuovo catalizzatore a base di rame

Per il nostro studio abbiamo deciso di sintetizzare un nuovo materiale in cui nanoparticelle di rame sono inglobate in una struttura carboniosa. Il progetto del catalizzatore si è basato su due idee principali.

Il primo spunto arriva dal lavoro di Shen et al., che hanno mostrato come confinare nanoparticelle di rame in nanocavità carboniose azotate permetta di intrappolare ioni OH^- generati in reazione, creando così un aumento locale del pH vicino ai siti attivi. Questa micro-alcalinità migliora la selettività e l'efficienza, portando a prestazioni paragonabili a quelle in elettroliti fortemente basici, ma partendo da un elettrolita neutro. Questo approccio può rivelarsi molto utile anche per la riduzione di CO_2 o CO, dove il pH locale influenza fortemente il legame degli intermedi e quindi i prodotti finali [35].

La seconda idea viene dal lavoro di Ferro et al., che descrivono un metodo per inserire nanoparticelle di platino nei pori di un supporto carbonioso [36].

Abbiamo quindi combinato i due concetti per ottenere un catalizzatore in cui nanoparticelle di rame sono inglobate nei pori del supporto carbonioso FCX650SE. La struttura e il meccanismo di funzionamento proposti sono illustrati in Fig. 15. Il nuovo catalizzatore sintetizzato sarà chiamato CuIN@FCX650SE all'interno di questa tesi.

II.II.I Sintesi del catalizzatore

Come precursore abbiamo usato nitrato di rame (II) emipentaidrato. È stato sciolto in 20 mL di acetone sotto agitazione magnetica, poi aggiunto il carbonio FCX650SE e infine 20 mL di acqua deionizzata. La miscela è stata agitata per 20 minuti e sonificata per altri 20 minuti in

bagno a ultrasuoni (CPX5800 Fisher) per ottenere una dispersione omogenea. Successivamente, la sospensione è stata essiccata in stufa ottenendo il materiale di partenza.

Infine, il composto secco è stato ridotto termicamente in un forno a tubo (Lindberg/Blue M) a 300°C per 2 ore sotto flusso di 5% H_2/95% Ar, trasformando gli ossidi di rame in rame metallico attivo.
Un sommario della preparazione del nuovo catalizzatore è illustrato in Fig. 16.

II.II.II Quantificazione del rame finale

Per determinare il contenuto di rame (% in peso) abbiamo usato la spettroscopia UV-Vis. Dopo la combustione del supporto carbonioso a 850 °C per 40 minuti, il rame rimasto, sottoforma di ossido rameoso, è stato sciolto in HCl concentrato e poi ridissolto in NH_4OH, formando un complesso blu intenso con assorbimento caratteristico a 640 nm (Fig.17).

La concentrazione è stata calcolata confrontando l'assorbanza con una curva di calibrazione costruita con soluzioni standard di $CuCl_2$ (Fig.18).

II.III Sintesi del catalizzatore tandem Cu/Ag

Durante i test iniziali, il catalizzatore CuIN@FCX650SE mostrava produzione di acetato nella riduzione di CO, ma non in quella di CO_2. Da qui abbiamo avuto l'idea di accoppiarlo con nanoparticelle di argento, note per l'elevata selettività nella conversione di CO_2 in CO, creando così un sistema tandem: dapprima si ha la riduzione della CO_2 in CO sui siti attivi dell'argento, successivamente si ha la riduzione del monossido di carbonio nei vari prodotti grazie all'azione del rame.

Per prepararlo, abbiamo miscelato quantità uguali in peso di CuIN@FCX650SE e nanoparticelle di Ag in 20 mL di acetone, lasciando agitare per tutta la notte. Il materiale è stato poi lavato tre volte con alcol isopropilico (IPA) tramite centrifugazione per rimuovere residui di surfattante (PVP), filtrato e infine essiccato in stufa. Una sintesi del procedimento è illustrata in Fig. 19. Tale catalizzatore sarà riferito come Cu/Ag@FCX650SE.

Tramite la stessa procedura, abbiamo anche preparato un catalizzatore con solo Ag su carbonio, chiamato Ag@FCX650SE.

II.IV Caratterizzazione del catalizzatore

Per caratterizzare il catalizzatore, abbiamo utilizzato principalmente due tecniche: la diffrazione a raggi X (XRD) e la microscopia elettronica a trasmissione (TEM). I principi di base di ciascun metodo sono brevemente descritti nei paragrafi seguenti.

II.IV.I Diffrazione a raggi X (XRD)

La diffrazione a raggi X è una tecnica molto potente per studiare la struttura cristallina, la composizione di fase e la dimensione media dei cristalliti di un materiale. Quando un campione cristallino viene irradiato con raggi X, gli atomi del reticolo cristallino causano la diffrazione della radiazione incidente a specifici angoli. Tali pattern di diffrazione seguono la legge di Bragg (Eq. 3) che mette in relazione la lunghezza d'onda dei raggi X (λ), la distanza interplanare (d) e l'angolo di diffrazione (θ). Analizzando i picchi di diffrazione, è possibile identificare le fasi cristalline presenti e stimare la dimensione media dei cristalliti tramite l'equazione di Scherrer. Nel nostro lavoro, la XRD è stata utilizzata per confermare la formazione di rame metallico dopo il processo di riduzione termica e per valutare il grado di cristallinità del catalizzatore finale [38].

II.IV.II Microscopia elettronica a trasmissione (TEM)

La microscopia elettronica a trasmissione permette di osservare direttamente i materiali su scala nanometrica e persino sub-nanometrica. In questa tecnica, un fascio di elettroni ad alta energia (tipicamente 100–300 keV) viene trasmesso attraverso un campione ultra-sottile. L'interazione degli elettroni con gli atomi del campione genera un contrasto che dipende dal numero atomico, dalla densità e dallo spessore, rivelando informazioni dettagliate sulla struttura e sulla morfologia. La TEM consente di ottenere dati sulla dimensione, forma e distribuzione delle particelle, e persino sull'orientazione cristallografica tramite la diffrazione da area selezionata (SAED). In questo studio, la TEM è stata utilizzata per caratterizzare la morfologia delle nanoparticelle di rame e la loro dispersione sul supporto carbonioso [39].

II.V Setup elettrochimico

Per i nostri esperimenti abbiamo utilizzato principalmente due configurazioni: H-Cell e Flow Cell.

- CO_2RR (riduzione della CO_2): testata in entrambe, usando come elettrolita una soluzione 0.2M di bicarbonato di potassio ($KHCO_3$).
- CORR (riduzione del CO): solo in Flow Cell, per la bassa solubilità del CO in acqua. Abbiamo variato il pH dell'elettrolita utilizzato per studiare l'effetto di questo parametro; abbiamo quindi testato 6 valori diversi di pH tra 8.5 (soluzione 0.2M di $KHCO_3$) e 13.5 (soluzione 1M di $KHCO_3$).

Le tecniche principali utilizzate nei due esperimenti sono riassunte di seguito:

- EIS per misurare la resistenza ohmica ed effettuare correzione iR.
- CV per valutare il comportamento redox e identificare potenziali attivi.
- CA per studiare stabilità e prestazioni a potenziale costante.
- Efficienza faradica (FE): calcolata confrontando la carica usata con quella necessaria a produrre i prodotti desiderati, calcolata secondo l'Eq. 5.

- Yield rate: quantità di prodotto per tempo e area attiva, calcolato utilizzando l'Eq. 6.

II.VI Quantificazione dei prodotti liquidi

Per quantificare la concentrazione dei prodotti liquidi generati durante i nostri esperimenti, abbiamo utilizzato due tecniche analitiche: la spettroscopia ^{1}H-NMR e la cromatografia liquida ad alte prestazioni (HPLC). Nei paragrafi seguenti vengono descritti brevemente i principi fondamentali di ciascun metodo.

II.VI.I Spettroscopia ^{1}H-NMR

La spettroscopia ^{1}H-NMR (Risonanza Magnetica Nucleare del protone) è una tecnica analitica utilizzata per identificare e quantificare le molecole organiche analizzando l'ambiente magnetico degli atomi di idrogeno (protoni) all'interno di un composto. Il metodo si basa sul fatto che i nuclei di idrogeno possiedono un momento magnetico e possono allinearsi parallelamente o antiparallelamente a un campo magnetico esterno. Quando viene applicato un impulso a radiofrequenza, i nuclei assorbono energia e passano a stati di spin eccitati. Tornando allo stato iniziale, emettono un segnale che viene rilevato e trasformato in uno spettro NMR. Lo spostamento chimico e la forma dei segnali forniscono informazioni dettagliate sulla struttura chimica, sui gruppi funzionali e sull'ambiente dei protoni nella molecola. Negli studi di elettroriduzione di CO_2 e CO, la ^{1}H-NMR è comunemente impiegata per identificare e quantificare prodotti liquidi come etanolo, acetato e formiato, spesso utilizzando standard interni per migliorare l'accuratezza [41].

II.VI.II Cromatografia liquida ad alte prestazioni (HPLC)

La cromatografia liquida ad alte prestazioni è una tecnica analitica fondamentale per separare, identificare e quantificare i componenti in miscele liquide. Il sistema è costituito da una pompa ad alta pressione che spinge il campione liquido attraverso una colonna riempita con una fase stazionaria, solitamente composta da particelle di piccole dimensioni. Durante il passaggio nella colonna, i componenti del campione interagiscono in modo diverso con la fase stazionaria in base alla loro polarità, dimensione o affinità chimica, venendo così separati. Ogni composto lascia la colonna con un tempo di ritenzione caratteristico e viene rilevato tramite rivelatori UV-Vis o a indice di rifrazione. L'HPLC è ampiamente utilizzata nella ricerca sulla riduzione elettrochimica della CO_2 per quantificare acidi organici a basso peso molecolare, come l'acido formico e l'acido acetico, difficilmente distinguibili con altre tecniche. Offre inoltre alta sensibilità, buona riproducibilità e la possibilità di analizzare specie non volatili o termicamente instabili [42].

II.VII Test sperimentali

II.VII.II Test sperimentali in H-Cell

I primi esperimenti sui catalizzatori a base di rame per la riduzione elettrochimica della CO_2, come nanoparticelle commerciali di rame (CuNPs) o CuNPs supportate su NiNC, sono stati condotti in configurazione H-Cell.

Per preparare gli elettrodi, i catalizzatori venivano dispersi in una miscela solvente per ottenere un inchiostro catalitico, poi depositato su carta di carbonio con un'area attiva di 1 cm^2. La ricetta era la seguente: 5 mg di catalizzatore, 670 µL di isopropanolo, 300 µL di acqua deionizzata e 30 µL di soluzione di Nafion. In totale, venivano depositati 100 µL di inchiostro per elettrodo, pari a un carico di 0,5 mg/cm^2 di catalizzatore.

Il protocollo di misura prevedeva inizialmente un'EIS per determinare la resistenza del sistema, seguita da una CV per valutare l'attività elettrochimica del catalizzatore. Successivamente venivano condotti esperimenti di CA a potenziali costanti compresi tra –0,6 V e –1,0 V vs. RHE, ciascuno della durata di un'ora. Si applicava inoltre una compensazione iR pari all'85% della resistenza misurata.

Al termine di ogni test di CA, l'elettrolita catodico veniva raccolto e sostituito con soluzione fresca. I campioni raccolti venivano analizzati tramite spettroscopia ^{1}H-NMR per identificare e quantificare i prodotti liquidi.

Tuttavia, le densità di corrente ottenute con l'H-cell risultavano piuttosto basse, e l'unico prodotto rilevato era il formiato. Per questo motivo, l'attenzione si è spostata verso l'uso di una flow cell, in grado di raggiungere densità di corrente più elevate. Inoltre, per la quantificazione dei prodotti si è preferito utilizzare l'HPLC, che offre limiti di rilevabilità più bassi e una maggiore sensibilità rispetto alla spettroscopia ^{1}H-NMR.

II.VII.II Test sperimentali in Flow Cell

Nella configurazione flow cell sono stati testati tutti i catalizzatori sintetizzati e quelli commerciali, sia per la riduzione della CO_2 che per quella del CO. I catalizzatori studiati includevano CuNPs commerciali e i nuovi materiali CuIN@FCX650SE, Ag@FCX650SE e Cu/Ag@FCX650SE.

Le misure elettrochimiche comprendevano inizialmente una CV, seguita da CA a tensioni di cella comprese tra –3 V e –5 V. In una flow cell, infatti, il potenziale applicato si indica solitamente come tensione complessiva della cella, e non rispetto a un elettrodo di riferimento come RHE, poiché si tratta di sistemi a due elettrodi separati da membrana, in cui conta la tensione totale necessaria a far procedere la reazione tra catodo e anodo.

Per preparare gli elettrodi si utilizzava questa ricetta: 25 mg di catalizzatore, 3 mL di IPA e 20 µL di Nafion. Di questa sospensione, 360 µL venivano depositati su un GDE, coprendo un'area

di 3 cm^2, per un carico nominale di 1 mg/cm^2. Tuttavia, l'area geometrica effettivamente esposta all'elettrolita era di 1 cm^2. Nel caso del CuIN@FCX650SE, si è aumentato il volume d'inchiostro a 540 µL, per incrementare il numero di siti attivi accessibili.

Il primo catalizzatore testato in flow cell sono stati le CuNPs commerciali. Con questi è stato condotto uno screening del pH per la riduzione di CO, al fine di valutare il ruolo del pH nel sistema. I valori di pH sono stati variati tra 8.5 e 13.5, utilizzando sei soluzioni diverse ottenute miscelando $KHCO_3$ 0.2 M (pH 8.5) e KOH 1 M (pH 13.5) in proporzioni variabili. Successivamente, lo stesso catalizzatore è stato testato anche per la riduzione della CO_2 in $KHCO_3$ 0.2 M.

Il secondo catalizzatore studiato è stato il nuovo CuIN@FCX650SE, testato a pH 8.5 per la riduzione del monossido di carbonio e successivamente la sua attività è stata valutata anche per la riduzione della CO_2 utilizzando lo stesso elettrolita

Infine, sono stati testati anche Ag@FCX650SE e Cu/Ag@FCX650SE per la riduzione della CO_2, sempre in $KHCO_3$ 0.2 M.

III. Risultati

III.I Caratterizzazione dei nuovi catalizzatori

In questo paragrafo vengono discussi i principali risultati della caratterizzazione dei nuovi catalizzatori tramite analisi XRD e TEM.

III.I.I Caratterizzazione di CuIN@FCX650SE

Nella sintesi del nuovo catalizzatore a base di rame CuIN@FCX650SE, l'obiettivo iniziale era ottenere un catalizzatore con il 30% in peso di rame seguendo la procedura illustrata in Fig. 16. Tuttavia, il carico di rame risultava eccessivo, causando la formazione di grandi aggregati che non riuscivano ad ancorarsi alla superficie del carbonio, come si osserva in Fig. 22.

Per ovviare a questo problema, la quantità di rame nel catalizzatore è stata ridotta, realizzando due test con un loading del 10% e del 15% in peso. La quantificazione del rame effettivamente presente, effettuata con il metodo descritto al capitolo 2.2.2, ha mostrato un contenuto finale pari al 5,44% per il campione con 10 wt% e al 13,41 wt% per quello con 15 wt%. Pertanto, per i test successivi è stato scelto il catalizzatore con il 15 wt%.

L'analisi TEM dei due campioni ci ha permesso di confrontarne la struttura su scala nanometrica (Fig. 23). A sinistra è mostrato il campione con 10% di rame, mentre a destra quello con 15%. Le macchie scure rappresentano le nanoparticelle di rame incorporate nella matrice carboniosa. Il catalizzatore con 10 wt% mostra una distribuzione scarsa e irregolare, coerente con i dati UV-Vis, mentre quello con 15 wt% presenta una distribuzione più uniforme, seppur con una certa variabilità nelle dimensioni.

Un ingrandimento (Fig. 24) evidenzia la morfologia delle nanoparticelle. In Fig. 24A la distribuzione appare abbastanza omogenea, mentre in Fig. 24B si osservano chiaramente le differenze dimensionali: le particelle più grandi raggiungono circa 30 nm, in linea con le nanoparticelle commerciali usate negli esperimenti preliminari di screening del pH.

Per identificare le fasi cristalline, è stata condotta un'analisi XRD confrontata con dati di letteratura (Fig. 25). Sono state individuate le principali fasi cristalline del rame: Cu (111), Cu (200), Cu (220), quest'ultima non riportata in figura [43]. Dal diffrattogramma risulta evidente la maggiore presenza di rame nel catalizzatore al 15 wt% rispetto a quello al 10 wt%.

III.I.II Caratterizzazione di Cu/Ag@FCX650SE

Per il catalizzatore contenente sia rame che argento, sono stati pesati 100 mg del materiale rame-carbonio, contenente 13,41 mg di rame, e miscelati con una quantità equivalente di nanoparticelle di argento commerciali. Il catalizzatore finale contiene quindi 11,82% in peso di entrambi i metalli.

L’analisi XRD ha permesso di identificare le fasi cristalline, confermando la presenza di rame e argento grazie al confronto con i dati di letteratura [43,44] (Fig. 26).

Le immagini TEM hanno mostrato la coesistenza delle due tipologie di nanoparticelle. In Fig. 27A si osservano le particelle di argento, di dimensione di circa 100 nm, ben distinguibili. In Fig. 27B è evidente la compresenza di rame e argento: le particelle di Ag si depositano sulla superficie carboniosa, mentre quelle di rame, più piccole, si inseriscono negli spazi tra i piani grafitici del supporto.

III.II Screening del pH con la riduzione di CO

Lo screening del pH per la CORR è stato condotto per individuare le condizioni ottimali di pH e voltaggio per massimizzare la produzione di Acetato e altri prodotti. Sono stati calcolati l’efficienza faradica e la velocità di produzione, riportate nei grafici seguenti.

Dai dati riassunti nei grafici di Fig. 28 si osserva che l’efficienza faradica per l’Acetato raggiunge il massimo a pH 13,5 (1 M KOH) per quasi tutti i voltaggi, tranne a −5 V, dove prevale la formazione di prodotti gassosi (Fig. 29). L’efficienza massima registrata è 23.54% a −3 V e pH 13.5. Il Formiato non si forma a causa dell’assenza dell’intermedio necessario partendo da CO, come visto in Fig. 4, mentre Etanolo e 1-Propanolo non mostrano tendenze nette rispetto al pH, ma dipendono fortemente dal voltaggio.

I grafici in Fig. 29 mostrano invece che i prodotti principali restano specie gassose (H_2, etilene, metano). L’Acetato spicca nettamente solo a pH 13.5, mentre l’etanolo è in generale il prodotto liquido più abbondante.

L’analisi dello yield rate in Fig. 30, infine, conferma che a pH 13.5 Acetato ed Etanolo raggiungono i valori massimi di resa molare. Per l’1-Propanolo invece la produzione rimane costante al variare del pH.

In conclusione, lo screening indica che le condizioni ottimali per la produzione di Acetato sono alto pH e bassa tensione, per limitare i prodotti gassosi. Tuttavia, tali condizioni non sono trasferibili alla CO_2RR, poiché la dissoluzione di CO_2 porta alla formazione di carbonati e bicarbonati che abbassano il pH.

III.III Confronto tra CuNPs e CuIN@FCX650SE

È stato eseguito un confronto tra nanoparticelle commerciali di rame (CuNPs) e il nuovo catalizzatore CuIN@FCX650SE in CORR, usando come elettrolita 0,2 M $KHCO_3$.

I risultati sintetizzati in Fig. 31 mostrano che CuNPs hanno prestazioni migliori per Etanolo e 1-Propanolo, mentre il nuovo catalizzatore risulta promettente per l’Acetato: a tensioni elevate (≥ 4 V) raggiunge efficienze più alte rispetto ai CuNPs, anche se mai oltre il 5%. Considerando che contiene solo il 13,41% di rame, il risultato è incoraggiante.

III.IIII Risultati di riduzione della CO_2

La riduzione di CO_2 è stata testata con quattro catalizzatori. Come mostra la Fig. 32, le nanoparticelle commerciali di rame hanno dato la prestazione migliore, con un massimo di 40,49% di efficienza faradica verso prodotti liquidi.

Le prestazioni peggiori sono state osservate con CuIN@FCX650SE e Ag@FCX650SE (FE~20%). Tuttavia, la combinazione dei due metalli in Cu/Ag@FCX650SE ha migliorato significativamente le performance, raggiungendo una efficienza faradica di 31.87% a −4 V.

In tutti i casi, il prodotto principale è stato il Formiato, mentre Etanolo e 1-Propanolo si formano in quantità ridotte e l'Acetato non è stato mai rilevato, confermando la difficoltà nel dirigerne la formazione in CO_2RR.

IV. Conclusioni e prospettive future

Questo lavoro ha esplorato e sviluppato catalizzatori a base di rame per la produzione selettiva di Acetato. Partendo dalla capacità intrinseca del rame di promuovere l'accoppiamento C–C nella riduzione di CO_2, sono stati progettati e sintetizzati nuovi sistemi catalitici:

- CuIN@FCX650SE, con nanoparticelle di rame inglobate in una matrice carboniosa grafitica.
- Cu/Ag@FCX650SE, un ibrido bimetallico rame–argento.

Gli esperimenti di CORR hanno evidenziato che condizioni fortemente alcaline (pH 13,5) e bassi voltaggi massimizzano la selettività verso Acetato, con un'efficienza faradica del 23.54% a −3 V. Tuttavia, queste condizioni non sono trasferibili alla CO_2RR a causa della formazione di carbonati e bicarbonati.

Nella CO_2RR, i CuNPs hanno raggiunto l'efficienza faradica più alta verso i prodotti liquidi (40,49%), mentre il catalizzatore Cu/Ag ha superato i singoli Cu o Ag, arrivando ad un'efficienza faradica totale del 31,87%. In tutti i casi, il Formiato è risultato il prodotto principale, con solo tracce di Etanolo e 1-Propanolo e nessuna formazione di Acetato.

Questi risultati sottolineano l'importanza della composizione del catalizzatore, della sinergia tra i siti attivi e del microambiente di reazione per orientare la selettività verso gli ossigenati multicarboniosi.

Le prospettive future includono:

- ottimizzare il contenuto di rame in CuIN@FCX650SE,
- calibrare il rapporto Cu:Ag in Cu/Ag@FCX650SE,
- esplorare la sintesi di leghe Cu–Ag vere e proprie per ridurre i limiti di trasporto di massa e controllare la diffusione degli intermedi.

In parallelo, l'ingegnerizzazione dell'elettrolita potrebbe aiutare a sviluppare sistemi catalitici più efficienti e vicini a un'applicazione industriale per la produzione sostenibile di Acetato.

1. **Introduction**

1.1 Climate change and CO_2 emissions

Climate change stands out as one of the most intricate challenges facing the modern world, involving environmental, economic, and social dimensions. A major factor contributing to this global issue is the continuous rise in atmospheric carbon dioxide (CO_2) levels, primarily linked to human activities such as fossil fuel combustion, deforestation, and industrial processes [1,2].

In recent decades, anthropogenic CO_2 emissions have consistently increased, surpassing 30 billion tons of carbon annually. Although a slight drop was observed during the COVID-19 pandemic, the overall upward trend has remained largely unchanged, as depicted in Fig. 1. This persistent increase in CO_2 has already driven global average temperatures to more than 1.1 °C above pre-industrial levels, an alarming shift with potentially irreversible consequences that could last for centuries [3].

Current climate projections indicate that, without significant and immediate mitigation efforts, global temperatures could rise by over 2 °C by the end of this century. Such a scenario would go well beyond the threshold set by the Paris Agreement in 2015, undermining international climate goals and increasing the likelihood of severe climate-related impacts worldwide [4].

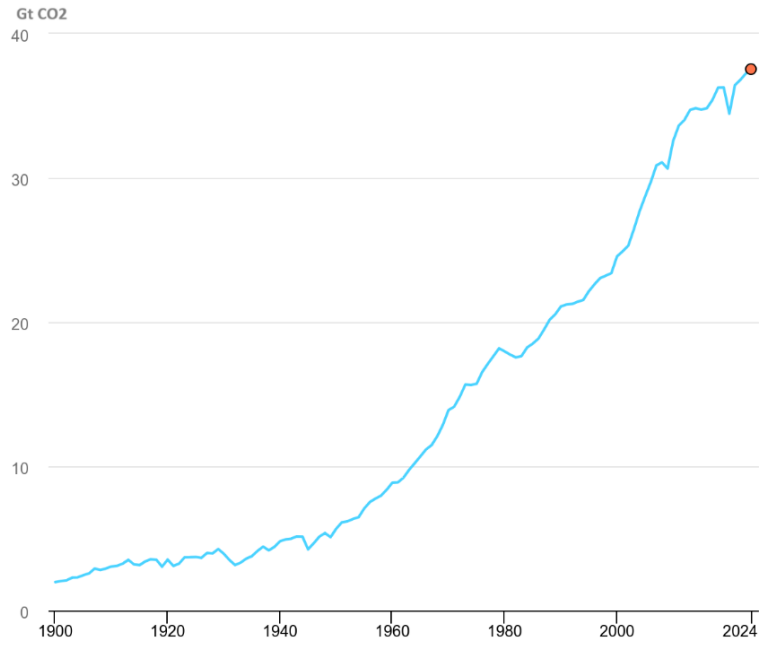

***Figure 1**: Global CO2 emissions from energy combustion and industrial processes and their annual change, 1900-2023 [3]*

The effects of global warming are already being felt across the planet, manifesting in rising sea levels, more frequent and intense extreme weather events, and widespread disruptions to natural ecosystems [5]. Tackling this crisis requires more than just awareness, it demands a deep

understanding of how CO_2 emissions are generated, where they come from, and how they influence the climate system. Concrete and effective actions must be taken to brake greenhouse gas emissions, and one of the most impactful strategies is to shift from fossil fuels to renewable energy sources [6].

Among the proposed technological solutions, carbon capture and storage (CCS) has received attention for its ability to reduce industrial CO_2 emissions by sequestering them underground. However, one major drawback of CCS is that it lacks economic incentive, as the captured carbon typically has no further use. In contrast, carbon capture and utilization (CCU) represents a more dynamic and potentially sustainable approach. Instead of simply storing CO_2, CCU technologies aim to transform it into valuable products, such as fuels, polymers, and industrial chemicals, thus combining environmental benefits with economic opportunity [7].

1.2 Electrochemical reduction of CO_2

The electrochemical reduction of carbon dioxide (CO_2RR) is increasingly recognized as a promising strategy to tackle some of today's environmental challenges. This approach relies on converting CO_2 into value-added products by using electrical energy, which can be supplied either through conventional power sources, such as a potentiostat in laboratory setups, or through renewable sources like solar panels and wind turbines in practical applications. When powered by clean energy, CO_2RR not only contributes to closing the carbon cycle but also provides a potentially carbon-negative route for the sustainable production of fuels and chemicals [8].

From a thermodynamic perspective, however, CO_2 reduction is inherently challenging. Carbon dioxide is the most oxidized form of carbon, making it a thermodynamically stable and chemically inert molecule under standard environmental conditions. This stability derives largely from the strength of the carbon–oxygen double bonds, which makes activation and reduction difficult without the assistance of a catalyst or the application of significant external energy [9]. Furthermore, in aqueous electrolytes, the CO_2 reduction reaction directly competes with the hydrogen evolution reaction (HER), which often reduces the faradaic efficiency of the process and diverts electrons away from the desired products.

Despite these limitations, electrochemical CO_2 reduction offers several distinct advantages over thermal or biological approaches. It allows for precise control of key reaction parameters such as electrode potential, current density, and pH, which can be tuned in real time to influence product distribution. Additionally, electrochemical systems are inherently modular and can be scaled down for decentralized applications. Perhaps most importantly, CO_2RR can be seamlessly integrated with intermittent renewable energy sources, providing an effective means of storing excess electricity in the form of high-energy molecules, thus helping to address one of the major limitations of solar and wind power [10].

A typical CO_2 electrolyzer consists of a cathode, where CO_2 is reduced; an anode, where water is oxidized (typically through the oxygen evolution reaction, OER); and an electrolyte, which enables ion transport between the electrodes. The configuration of the electrochemical cell,

whether an H-type cell, a flow cell, or another design, plays a crucial role in determining overall performance in terms of efficiency, stability, and scalability.

Among all the factors that influence CO_2RR, the catalyst is arguably the most critical. The catalytic surface is responsible not only for activating the CO_2 molecule, which is itself a challenging step, but also for stabilizing reaction intermediates and guiding the reaction toward specific products. Over the past decade, considerable research has focused on developing and optimizing a wide variety of catalytic materials, including pure metals, metal oxides, and hybrid systems. Each of these material classes exhibits distinct activity, selectivity, and stability profiles. Notably, copper (Cu) has drawn significant attention due to its exceptional versatility, as it is the only metal known to effectively facilitate the formation of multi-carbon (C_2^+) products. These include not only formic and acetic acid but also short-chain alcohols such as Methanol, Ethanol, and Propanol, making Cu-based catalysts highly attractive for energy and chemical applications [11].

1.3 Thermodynamic aspects of CO_2 reduction

Carbon dioxide is known for being an exceptionally stable molecule, both from a thermodynamic and kinetic point of view. Its linear structure, made up of two strong double bonds between carbon and oxygen atoms (Fig. 2), and its fully occupied valence shell make it largely unreactive under standard ambient conditions. The strength of each carbon=oxygen double bond, with a bond enthalpy of around 750 kJ/mol, explains why considerable energy input is required to break these bonds and initiate a chemical transformation. As a result, activating and reducing CO_2 typically demands either high temperatures or the application of significant electrical energy in the form of an overpotential [12,13].

In electrochemical systems, the overpotential refers to the extra voltage that must be applied beyond the theoretical thermodynamic potential in order to drive the desired reaction. This additional energy compensates for kinetic limitations, sluggish intermediate formation, and the energy required to overcome the molecule's inherent resistance to change. In the case of CO_2 reduction, overpotentials can vary widely depending on the catalyst, the reaction environment, and the specific product targeted.

***Figure 2**: CO_2 structure*

From a thermodynamic point of view, the standard Gibbs free energy (ΔG^0) for CO_2 reduction is positive for most of the reaction products, meaning that the reactions are non-spontaneous and require external energy.

The general form of the reduction reaction is the following:

$$xCO_2 + nH^+ + ne^- \rightarrow product + yH_2O \quad (1)$$

All the main reactions that we can have in our system are reported in Tab. 1 [14].

***Table 1**: List of the main reactions involved in the CO2 reduction [14]*

Reaction	E°/ (V vs RHE)	(Product) Name
$2H_2O \rightarrow O_{2(g)} + 4H^+ + 4e^-$	1.23	Oxygen evolution reaction
$2H^+ + 2e^- \rightarrow H_{2(g)}$	0	Hydrogen evolution reaction
$CO_2 + 2H^+ + 2e^- \rightarrow HCOOH_{(aq)}$	-0.12	Formic acid
$CO_2 + 2H^+ + 2e^- \rightarrow CO_{(g)} + H_2O$	-0.10	Carbon monoxide
$CO_2 + 6H^+ + 6e^- \rightarrow CH_3OH_{(aq)} + H_2O$	0.03	Methanol
$CO_2 + 8H^+ + 8e^- \rightarrow CH_{4(g)} + H_2O$	0.17	Methane
$2CO_2 + 8H^+ + 8e^- \rightarrow CH_3COOH_{(aq)} + 2H_2O$	0.11	Acetic acid
$2CO_2 + 12H^+ + 12e^- \rightarrow C_2H_5OH_{(aq)} + 3H_2O$	0.09	Ethanol
$3CO_2 + 18H^+ + 18e^- \rightarrow C_3H_7OH_{(aq)} + 5H_2O$	0.10	Propanol

The reported E° is called standard electrode potential, it is a measure of a chemical species to gain electrons and be reduced. It is measured under standard conditions, which are 1M concentration for solutions, 1 atm pressure for gases, and a temperature of 298K. The reversible hydrogen electrode (RHE) is used as a reference and it has an assigned potential of 0 V; if our reaction has a E° > 0 the species tents to reduce, so to gain electrons, if our reaction has a E°<0 the species tents to oxidize, so to lose electrons.

These thermodynamic values indicate that producing simpler molecules like carbon monoxide or formic acid from CO_2 is generally more favorable than forming more complex, multi-electron products such as methanol or methane. However, these standard potentials don't tell us everything. They assume ideal conditions and do not consider the kinetic limitations, the need to stabilize reaction intermediates, or the actual energy input required under real operating conditions.

In practice, the overpotential needed to drive CO_2 reduction can be quite significant. Take carbon monoxide, for example: although its theoretical reduction potential is just –0.11 V versus the standard hydrogen electrode, in real systems it often takes between –0.5 and –1.0 V vs RHE to achieve appreciable reaction rates. This discrepancy is due to several factors, including slow reaction kinetics, inefficient adsorption of intermediates, and the energy required to couple proton and electron transfers effectively.

For this reason, thermodynamics alone cannot predict how well CO_2 reduction will work in a practical setting. The actual performance is heavily influenced by the choice of electrocatalyst, the local pH near the electrode surface, how efficiently CO_2 is delivered to the reaction site, and the design of the electrochemical cell itself. Overcoming the energy penalties associated with CO_2 activation means developing catalysts that not only lower the required overpotential, but also guide the reaction toward desired products while minimizing unwanted side reactions [15].

1.4 The role of Copper in CO_2 reduction

Catalysts used for CO_2 electroreduction can generally be grouped into four classes, based on their selectivity and activity. The first includes materials such as silver (Ag) and gold (Au), which are highly selective toward carbon monoxide production. The second class consists of metals like lead (Pb), mercury (Hg), and indium (In), which predominantly generate Formate ($HCOO^-$). A third group comprises those metals that show little to no activity toward CO_2 reduction, instead favoring the hydrogen evolution reaction; typical examples include platinum (Pt) and iron (Fe). Lastly, there is a fourth category, occupied only by copper (Cu), which stands apart for its ability to produce a wide spectrum of hydrocarbons and oxygenated products [14].

This unique position makes copper particularly important in the context of CO_2 electroreduction. Unlike most other metals, copper can go beyond simple two-electron transfers and mediate more complex reactions involving multiple proton and electron steps. This capability allows for the formation of carbon–carbon (C–C) bonds and ultimately the generation of multi-carbon (C_2^+) molecules, which are of significant industrial interest.

What gives copper this versatility is its intermediate binding strength with key carbon-containing intermediates. For instance, copper binds adsorbed *CO more strongly than gold or silver, which helps to retain it on the surface for further reaction steps, but not so strongly that it becomes trapped and deactivates the catalyst [16]. This delicate balance allows copper to stabilize a variety of intermediates, such as *CO, *CHO, and *OCCO, all of which are believed to play critical roles in C–C coupling and multi-carbon product formation [17]. (* stands for adsorbed species)

Copper's ability to produce C_2^+ products is especially relevant for two main reasons. First, these molecules are more energy-dense than simpler C_1 species and have larger commercial applications. Second, their synthesis requires the coupling of two carbon atoms, a step that is both thermodynamically unfavorable and kinetically demanding, making it a considerable challenge in catalysis [18].

Nevertheless, copper is not without limitations. One of the main issues is its lack of product selectivity, in fact, standard polycrystalline copper electrodes often produce a complex mix of reaction products, which complicates purification and limits overall efficiency. Moreover, copper typically requires relatively high overpotentials to drive the reaction, meaning more energy must be supplied to sustain CO_2 conversion, resulting in lower energy efficiency and higher operational costs [19].

For these reasons, significant research efforts have focused on engineering copper-based materials to overcome these limitations. Strategies include nanostructuring, oxide-derivation, alloying, and surface modification, all aiming to enhance selectivity, reduce overpotentials, and stabilize catalytic performance over time.

In summary, copper remains the benchmark catalyst for CO_2 electroreduction, especially for the production of hydrocarbons and alcohols. While it is far from perfect, its unmatched ability to support the formation of complex multi-carbon products has made it both a valuable research

model and a promising candidate for real-world applications. A deeper understanding of how copper interacts with CO_2 and its intermediates is essential for advancing toward efficient, scalable, and economically viable CO_2 conversion technologies.

1.5 CO_2 reduction pathways

Although significant progress has been made through both experimental studies and theoretical modeling, the reaction mechanism behind electrochemical CO_2 reduction is still not fully understood. One of the main reasons for this is the inherent complexity of the process: it involves a network of competing reaction pathways, numerous surface-bound intermediates, and a high sensitivity to several variables, including the structure of the catalyst surface, the local pH near the electrode, and the composition of the electrolyte. On top of that, catalyst surfaces tend to undergo structural and chemical changes during operation, which makes it even more challenging to pinpoint the actual active sites and to track how intermediates form and evolve under realistic conditions.

1.5.1 Pathway to C_1 products

Among the various reaction pathways investigated in CO_2 electroreduction, those leading to carbon monoxide (CO) and Formate ($HCOO^-$) are among the most established and extensively studied, as they involve only two-electron transfers and are more accessible from a thermodynamic and kinetic perspective.

The pathway toward CO generally proceeds through the formation of a surface-bound *COOH intermediate. After CO_2 adsorption, a first proton-coupled electron transfer (PCET) step forms *COOH, which is then reduced to *CO and subsequently desorbed from the catalyst surface as CO gas (Fig. 3). This mechanism is particularly favored on noble metals such as Au and Ag, due to their weak *CO binding energies, which allow easy desorption and high selectivity [20].

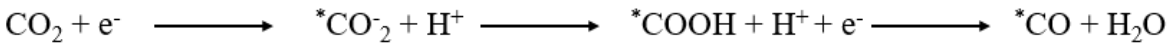

***Figure 3**: CO2 reduction to CO mechanism*

In contrast, the Formate pathway involves the formation of an *OCHO intermediate, in which the protonation occurs at one of the oxygen atoms of the CO_2 molecule. This intermediate is then protonated and released as $HCOO^-$ (Fig. 4). Metals like Bi, Sn, In, and Pb show high selectivity toward this pathway, as their surfaces stabilize *OCHO more effectively than *CO. Importantly, these two mechanisms tend to be mutually exclusive: catalysts that favor *COOH formation rarely stabilize *OCHO efficiently, and vice versa.

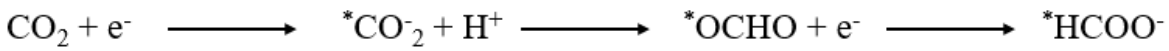

***Figure 4**: CO2 reduction to Formate mechanism*

Understanding these mechanisms is not only important for optimizing CO and Formate production, but also because CO serves as a key intermediate in the formation of more complex C_2^+ products on copper and related materials [14]. For this reason, clarifying the competition between these elementary steps is fundamental for the rational design of selective and efficient CO_2RR electrocatalysts.

1.5.2 Pathway to Ethanol and 1-Propanol

The electrochemical formation of alcohols such as Ethanol (C_2H_5OH) and 1-Propanol (C_3H_7OH) from CO_2 is of particular interest due to the high energy density and commercial relevance of these products. However, these reactions are mechanistically more complex than those leading to C_1 products, as they involve multiple proton-coupled electron transfer steps and, crucially, the formation of carbon–carbon (C–C) bonds.

The formation of Ethanol is widely believed to proceed through a *CO dimerization pathway. Initially, two *CO species adsorbed on adjacent active sites undergo coupling to form a *CO–CO intermediate, which is subsequently reduced to a surface-bound *OCCO species. Further protonation and electron transfer steps lead to a series of intermediates, including *OCCHO and $*CH_2CHO$, which are key precursors for Ethanol formation [17]. One proposed route involves the hydrogenation of $*CH_2CHO$ to $*CH_3CHO$ (acetaldehyde), which can be further reduced to Ethanol via the intermediate $*CH_3CH_2O$ (Fig 5). Alternatively, direct protonation of $*CH_2CHO$ may yield Ethanol without the need for a free aldehyde intermediate [21].

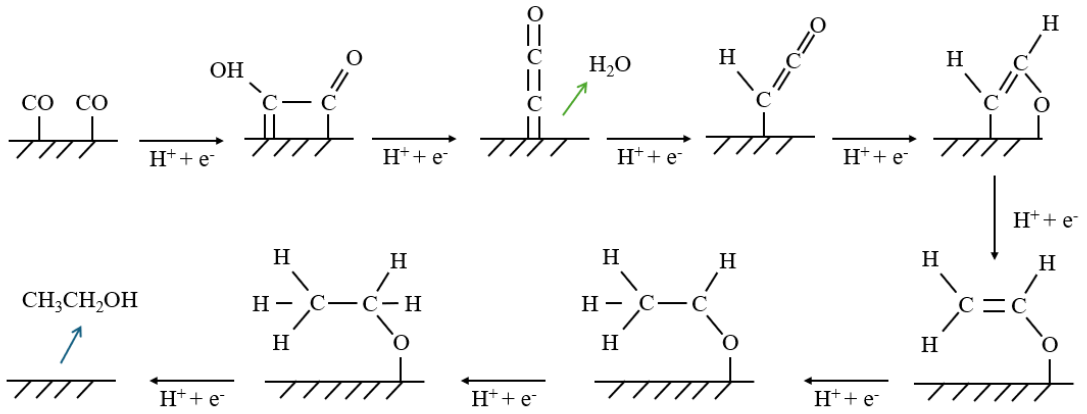

***Figure 5**: CO2 reduction to Ethanol mechanism [17]*

The formation of 1-Propanol, a C_3 alcohol, requires an additional carbon–carbon coupling step beyond that needed for Ethanol. This may occur through the nucleophilic attack of a surface-bound *CO onto a pre-formed $*CH_2CHO$ or $*CH_3CH_2O$ intermediate, forming a three-carbon $*C_3H_7O$ precursor (Fig. 6) [22].

The low faradaic efficiency typically observed for C_3 products reflects the kinetic difficulty of the additional C–C coupling step and the competitive nature of parallel pathways such as ethylene or Ethanol formation.

Overall, while the formation of Ethanol and 1-Propanol demonstrates the remarkable potential of copper-based catalysts to mediate complex multi-carbon reactions, further mechanistic clarity is needed. A deeper understanding of intermediate stabilization, active site structure, and electrolyte effects will be crucial for rationally enhancing the selectivity and yield of these valuable alcohols.

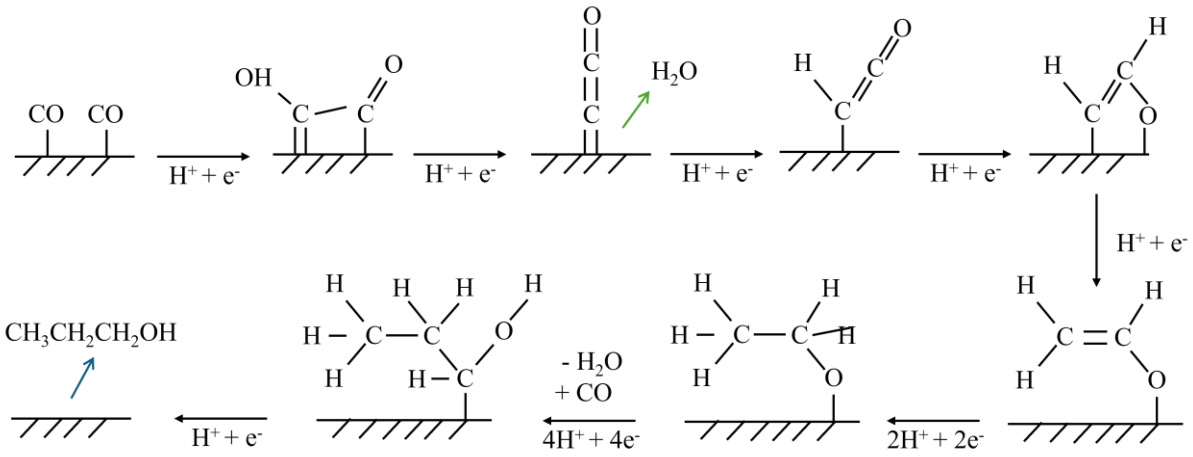

***Figure 6**: CO2 reduction to 1-Propanol mechanism*

1.5.3 Pathway to Acetate

The reaction pathway leading to Acetate formation is still not fully understood and remains an active area of investigation. However, recent studies based on computational methods, particularly density functional theory (DFT), have proposed possible mechanisms. One of the most recent and promising pathways starts not with the traditional *CO dimerization, but rather with a reaction between *CO and a surface-adsorbed hydroxide ion (*OH). This initial step leads to the formation of *COOH. Only afterward the system undergo carbon–carbon coupling, involving a second adsorbed *CO molecule, resulting in the intermediate *COCOOH. From this point, a series of PCET steps ultimately yields Acetate (Fig. 7) [23].

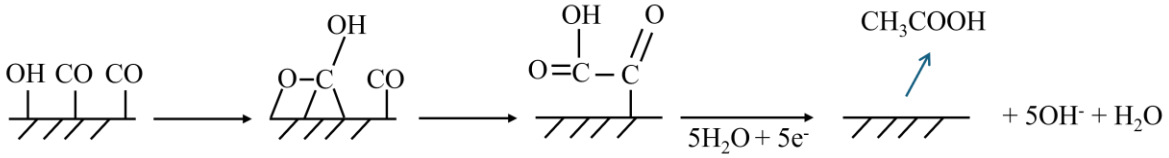

***Figure 7**: CO2 reduction to Acetate pathway [23]*

What stands out in this mechanism is the key role played by two adsorbed species: carbon monoxide and hydroxide ions. This means that for the pathway to proceed efficiently, a high *CO coverage is needed, along with a good availability of *OH on the surface. The latter can be promoted by increasing the pH of the electrolyte. However, this approach presents a challenge when the starting feedstock is CO_2, because at high pH, CO_2 readily reacts with

hydroxide to form carbonate (CO_3^{2-}) or bicarbonate ions (HCO_3^-), that are inactive species, which reduces the amount of CO_2 available for reduction.

This explains why reducing CO to Acetate is typically much easier than reducing CO_2 directly. With CO as the feed, *CO coverage is naturally higher, and it becomes possible to operate in a more alkaline environment, for example, using a 1 M KOH solution, without the same drawbacks.

Based on this reasoning, we explored the design of a new catalyst capable of retaining hydroxide ions near its surface. The idea is to locally increase the pH, creating favorable conditions for Acetate production, while avoiding the negative effects of bulk alkalinity on CO_2 availability. This concept will be discussed in more detail in the following chapters.

1.6 Electrolyzers for CO2RR

1.6.1 H-Cell

In CO_2 electroreduction research, the H-type cell remains one of the most widely used setups for fundamental studies, thanks to its simplicity and versatility. Structurally, an H-cell consists of two liquid-filled compartments, one cathodic and one anodic, separated by an ion-exchange membrane, providing an H shape. At the cathode we have the CO_2 reduction, while at the anode we have the Oxygen Evolution Reaction (OER). The ion-exchange membrane that we used in our system is Nafion that allows the ions to go from the cathode to the anode. A schematic representation and the real H-cell can be seen in Fig. 8.

The liquid product can be collected directly from the cathodic chamber, while the gas that exits from that side could be sent to a gas chromatograph to analyze the gaseous products.

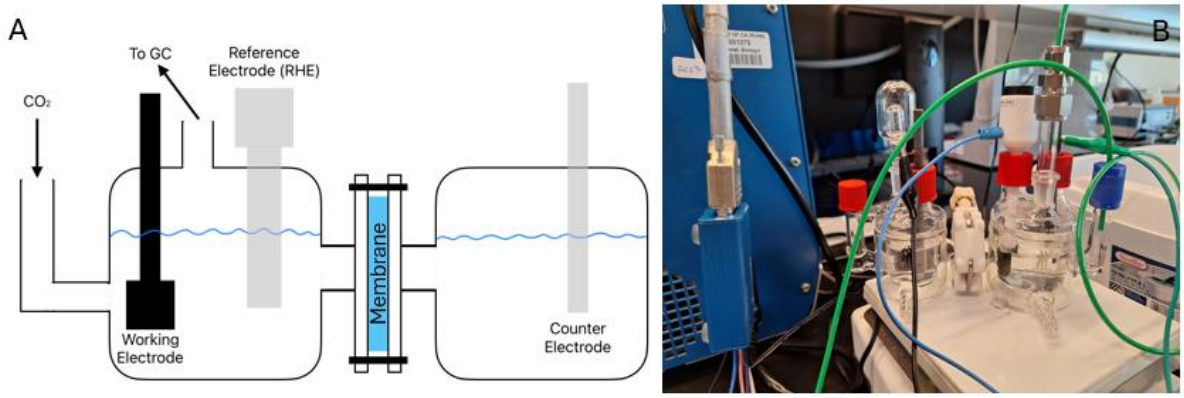

***Figure 8**: Schematic diagram of conventional H-Cell (A) and real image of the H-Cell (B)*

From an experimental standpoint, H-cells are popular because they are easy to assemble, inexpensive, and allow straightforward modifications to test various catalysts and operating

conditions. These features make them ideal for early-stage screening and performance benchmarking. However, H-cells are not without limitations. The biggest one among them is the poor mass transfer of CO_2, as its low solubility (about 33 mM at 1 atm and 25°C) in aqueous electrolyte severely restricts reaction rates. In practice, this results in low current densities and limited product formation; due to this we have to perform the electrochemical experiment for a long period of time, to reach the detection limit of the products.

Moreover, the small interfacial area between gas, liquid, and catalyst further hampers scalability, often rendering H-cells impractical for industrial application. While they excel in enabling reproducible and controlled experimentation, their design does not support continuous operation or high-throughput CO_2 conversion. These shortcomings have prompted the field to increasingly adopt flow cells and gas-diffusion electrode systems, which overcome many of the mass-transfer and surface-area constraints inherent in H-cell setups [24].

Despite these drawbacks, H-cells continue to play a crucial role in CO_2RR research. Their simplicity and analytical clarity ensure they remain a go-to option for shedding light on catalyst behavior, mechanistic pathways, and electrolyte effects, foundational knowledge that informs the design of more advanced reactor systems.

1.6.2 Flow Cell

In recent years, flow cells have emerged as a more advanced alternative to traditional H-type cells for electrochemical CO_2 reduction, particularly when aiming to achieve industrially relevant current densities and productivities. The defining feature of a flow cell is its continuous operation: gaseous CO_2 and liquid electrolyte are continuously fed into the system, allowing for higher throughput and more efficient mass transport. Typically, a flow cell includes a gas-diffusion electrode (GDE) at the cathode, a flowing liquid electrolyte, and an anode compartment separated by an ion-exchange membrane. A GDE typically consists of a porous, hydrophobic backing layer that allows CO_2 gas to diffuse through it, and a catalyst layer on the front side, which is in contact with the liquid electrolyte. This design creates a so-called three-phase boundary, where gas, liquid, and solid (catalyst) meet, an essential condition for fast and efficient electrochemical reactions. This configuration enables the direct delivery of CO_2 gas to the catalyst surface, which significantly overcomes the mass transport limitations associated with the low solubility of CO_2 in aqueous media [25]. A schematic diagram of the flow cell is represented in Fig. 9.

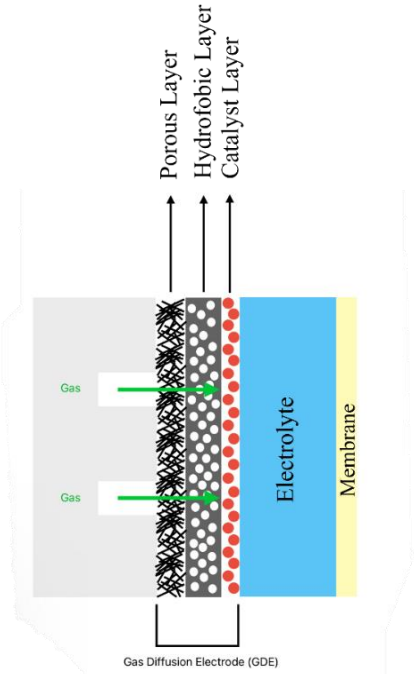

***Figure 9**: Schematic representation of the flow cell*

All the layers of the flow cell that we used for the experiment can be seen in Fig. 10A [26], along with an image of the electrolyzer used for the experiments (Fig. 10B). In the real image we can see the pump used for the liquid electrolyte, that takes the liquid from two vials filled with 15 mL of the electrolyte.

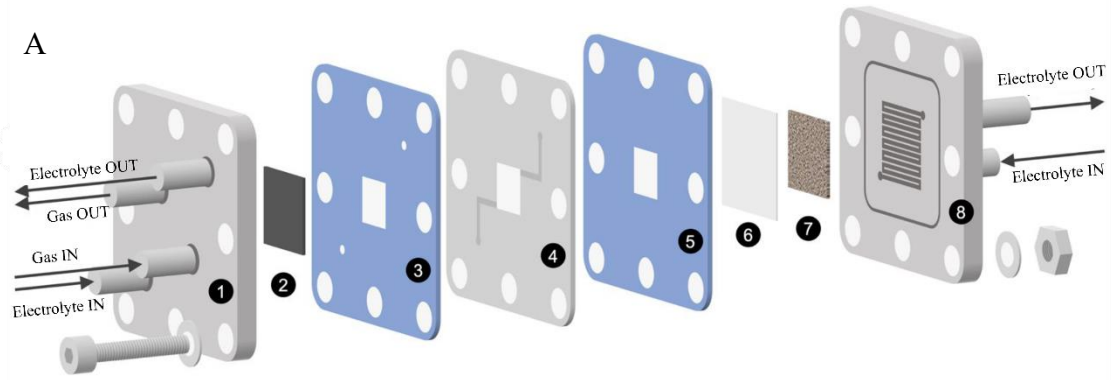

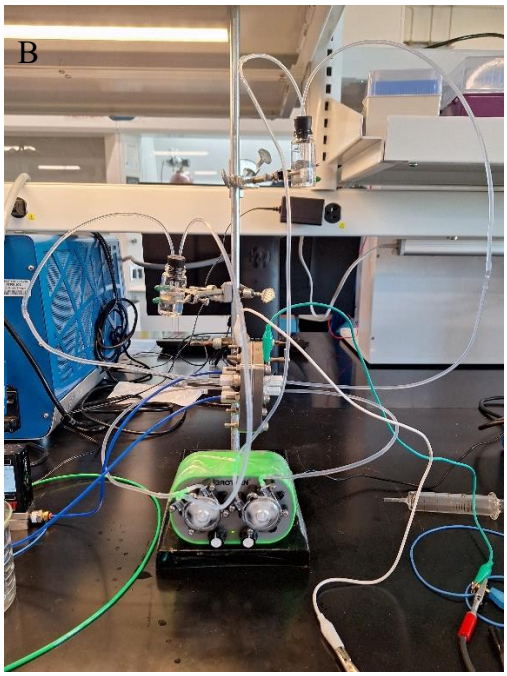

***Figure 10**: Schematic diagram of the flow cell and real image*

Figure 10A: Schematic diagram of the flow cell. ①, ⑧: Titanium flow plate; ②: Cu-GDE cathode; ③, ⑤: Silicone rubber gasket; ④: Middle flow channel; ⑥: Nafion membrane; ⑦: Nickel foam anode. [26] Figure 10B: Image of the flow cell used for the experiments.

Because of this improved CO_2 availability, flow cells can sustain much higher current densities, often exceeding 200 mA cm^{-2}, while still maintaining decent selectivity toward desired products. Moreover, the continuous nature of the system allows better control over gas–liquid–solid interfaces, reduced diffusion layer thickness, and enhanced Faradaic efficiencies. This makes flow cells a more practical platform for scaling up electrochemical CO_2 conversion, especially when integrated with renewable energy sources [27].

However, the benefits of flow cells come with trade-offs. The design and operation are more complex than H-cells, requiring precise control over gas and liquid flows, as well as careful management of flooding or drying in gas-diffusion electrodes. Long-term stability is another ongoing challenge: catalyst degradation, electrolyte crossover, and membrane fouling can limit continuous operation. Furthermore, while gas-diffusion layers allow CO_2 access, they also create challenges in maintaining triple-phase boundaries where CO_2, electrolyte, and catalyst all interact effectively.

Despite these challenges, flow cells are currently regarded as the most promising architecture for bridging the gap between laboratory-scale research and real-world application. Their modular design makes them compatible with stackable reactor systems, and ongoing innovations in membrane materials, electrode design, and electrolyte optimization continue to push the boundaries of CO_2RR performance in flow cell platforms [28].

1.7 Market Potential and Applications of Key Products from CO_2 Electroreduction

In this paragraph, we will briefly explore the main applications and market value of the key products that can be obtained through the electrochemical reduction of carbon dioxide and carbon monoxide.

1.7.1 Formic Acid

Formic acid is among the simplest products formed via the two-electron electrochemical reduction of CO_2. It has long-standing industrial applications in leather tanning, textile dyeing, and as a preservative in silage and animal feed. More recently, formic acid has gained interest as a liquid hydrogen carrier in low-temperature fuel cell systems, due to its high volumetric hydrogen density and ease of handling [29]. According to a market report by Precendence Research, the global formic acid market was $2.32 billion USD in 2024 and it is expected to increase to $3.78 billion USD in 2034 (Fig. 11) [30].

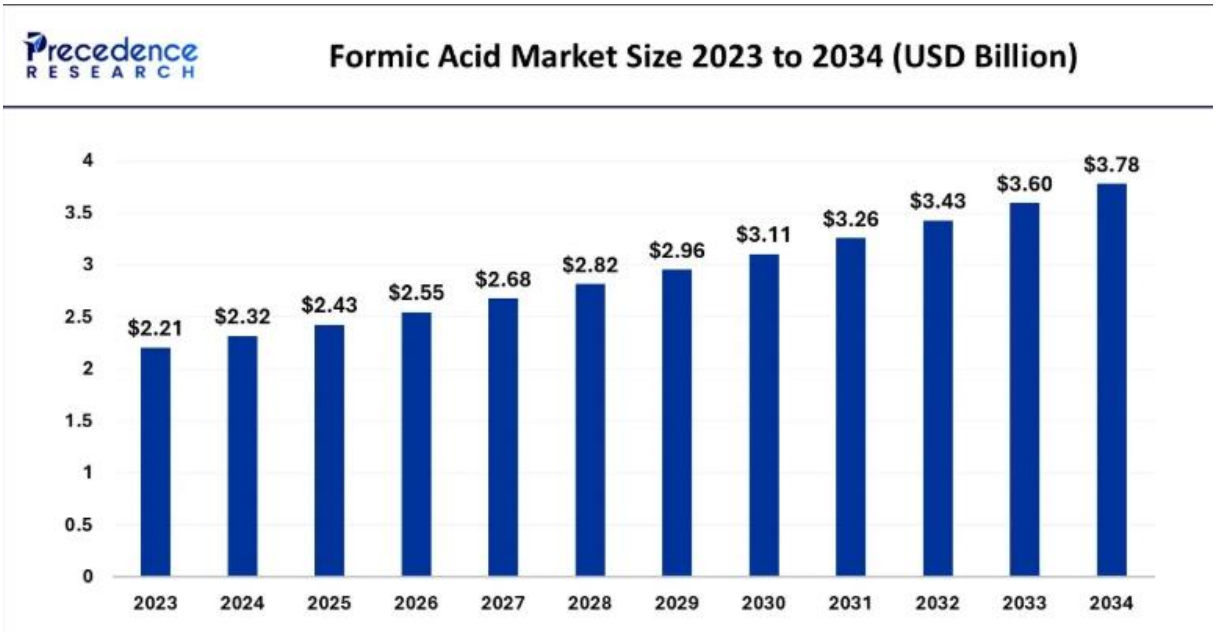

***Figure 11**: Formic acid worldwide Market Size [30]*

1.7.2 Acetic Acid

Acetic acid largest industrial application is in the production of vinyl Acetate monomer (VAM), which is used in adhesives, paints, and packaging materials. It also finds widespread use in food preservation, pharmaceuticals, and plastic manufacturing. As of 2023, the global acetic acid market was valued at approximately $13.8 billion USD and it is expected to grow to $23.02 billion USD by 2030 [31].

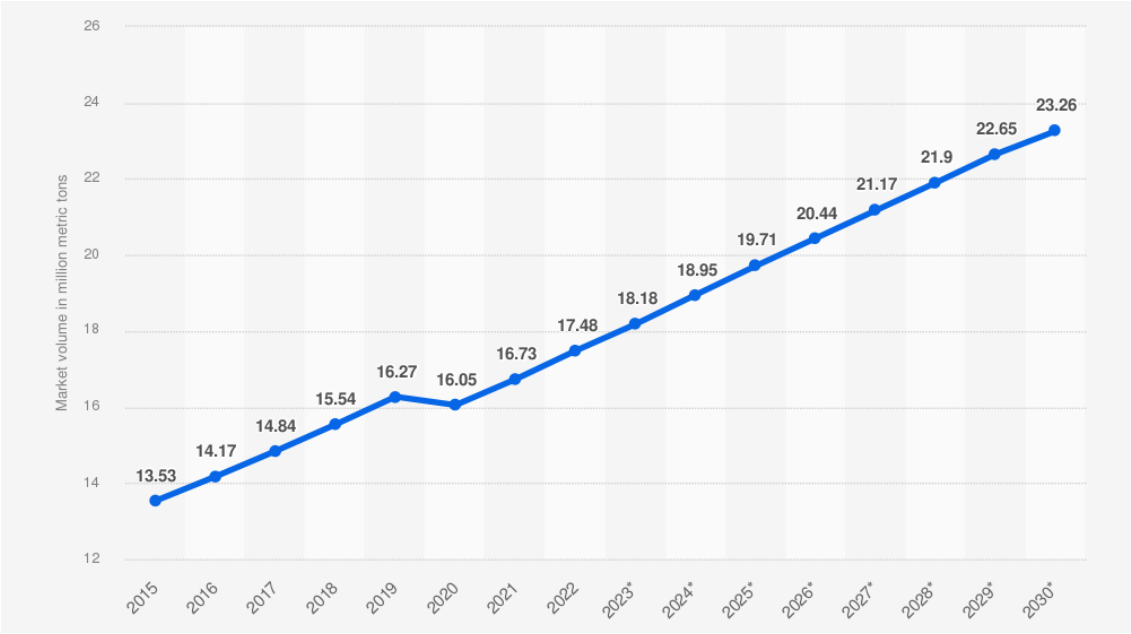

***Figure 12**: Market volume of acetic acid worldwide from 2015 to 2022, with a forecast for 2023 to 2030 (in milion metric tons) [31]*

1.7.3 Ethanol

Ethanol is one of the most sought-after liquid fuels from CO_2RR due to its high energy density and compatibility with existing fuel infrastructure. It is extensively used in pharmaceuticals, cosmetics, and as a solvent in chemical industries. While global Ethanol production is still dominated by bio-based fermentation, particularly from corn and sugarcane, electrochemical synthesis from CO_2 offers a carbon-neutral alternative that avoids land-use competition [32]. The global Ethanol market was valued at over $90 billion USD in 2023 and continues to grow due to energy transition policies and demand for cleaner fuels (Fig. 13) [33].

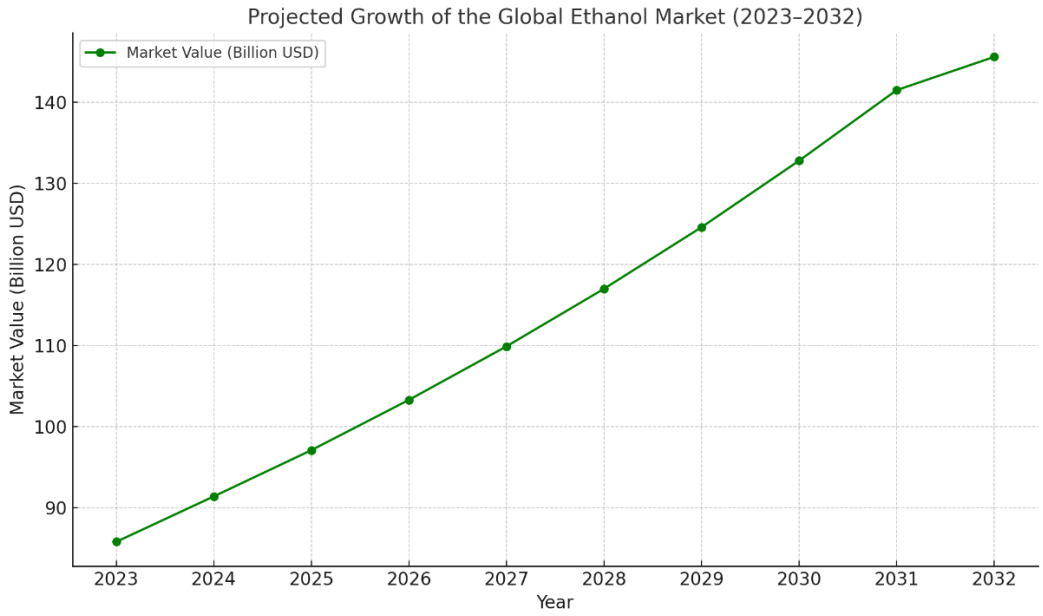

***Figure 13**: Projected Growth of the Global Ethanol Market [33]*

1.7.4 1-Propanol

1-Propanol is a higher alcohol with uses as a solvent, especially in coatings, printing inks, and pharmaceutical formulations. It is also a potential fuel and intermediate in chemical synthesis. While the global market for 1-Propanol is relatively small, estimated at $215.5 million USD in 2023 (Fig. 14), its selective electrochemical synthesis is of high interest due to the challenge of forming C_{3+} products from CO_2 [34]. Its successful production would mark a major milestone in the development of carbon-neutral fuels and specialty chemicals.

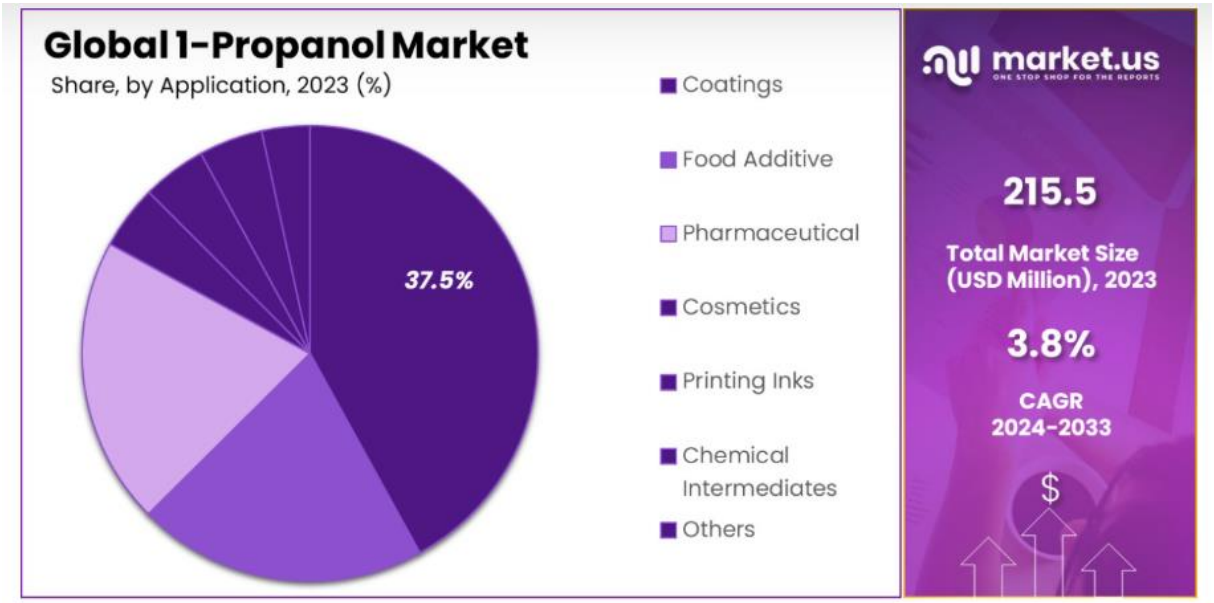

***Figure 14**: 1-Propanol Worldwide Market [34]*

1.8 Objectives

The main objective of this thesis is to better understand the catalytic behavior of copper in the electrochemical reduction of carbon dioxide and carbon monoxide. Special attention is given to the role of the electrolyte environment, especially the effect of pH, in modulating the activity and stability of key intermediates during CO_2 and CO reduction. In addition to investigating the fundamental catalytic mechanisms, this thesis also aims to explore the synthesis of a novel copper-based catalyst designed to enhance the selectivity toward acetic acid, a valuable multi-carbon product. By combining experimental work with insights from recent literature, the goal is to contribute to the development of more efficient and selective catalytic systems for carbon utilization in future energy technologies.

2. Experimental setup

2.1 Chemicals

Copper(II) nitrate hemi(pentahydrate) (purity ≥ 98%), Copper nanoparticles (TEM size = 25 nm), Silver Nanoparticles (TEM size ≤ 100 nm), Potassium Bicarbonate (purity ≥ 99.7%), Deuterium Oxide (D_2O, 99.8% atom D), Dimethyl sulfoxide-d6 (DMSO) and Nafion perfluorinated resin solution 5 wt. % were purchased from Sigma-Aldrich (USA). Potassium hydroxide (purity ≥ 85.0%) was purchased from MG scientific (USA). Isopropanol (IPA, purity ≥ 99.9%), Acetone (purity ≥ 99.5) and hydrochloric acid (36.5 to 38 wt. %) were purchased from Fisher Chemical (USA). Ammonium Hydroxide (28 to 30 wt. %) was purchased by VWR (USA). FCX650SE was purchased from Cabot (USA). CO (purity ≥ 99%) was purchased from Praxair (USA). CO_2 (purity ≥ 99.5%) and H_2 and Ar (5% H_2, 95% Ar) were purchased from AirGas (USA). Deionized ultrapure water (DIW) was obtained using a Millipore Milli-Q system (product water conductivity at 25 °C = 0.056 μS cm^{-1}).

2.2 A novel copper catalyst

For our research on copper-based catalysts, we decided to synthesize a new material featuring copper nanoparticles embedded within a carbon structure. The design of this catalyst was guided by two main ideas, which will be outlined in the following sections.

A particularly interesting strategy to enhance catalytic performance in electrochemical reactions has been presented by Shen et al., who developed an encapsulated copper catalyst capable of locally increasing the pH near the active sites, despite operating in a neutral bulk electrolyte. In their work, copper nanoparticles were confined inside nitrogen-doped hollow carbon nanocages, a structure that effectively traps hydroxide ions (OH^-) generated during the cathodic reaction. This confinement leads to a localized rise in pH around the copper surface, creating a favorable microenvironment for the electroreduction of nitrate and nitrite to ammonia. Remarkably, this local alkalinity allows the system to achieve a faradaic efficiency close to 100% and high production rates in conditions that would otherwise require a strongly alkaline electrolyte. The study demonstrates how modifying the catalyst's local environment, rather than altering the entire electrolyte, can significantly influence selectivity and reaction kinetics. This concept of self-enhanced localized alkalinity could be particularly useful in CO_2 or CO reduction, where local pH plays a critical role in determining the binding strength of key intermediates and the overall product distribution [35].

The second idea is based on the paper by Ferro et al., in which they talk about a methodology to put Platinum nanoparticles inside the pores of a carbon support [36].

We then tried to mix these two ideas together to make a new catalyst that has copper nanoparticles inside the pores of a carbon support, hoping we could have a result similar to the work by Shen et al. increasing the pH only near the surface of the catalyst. The structure and the proposed working mechanism of the new catalyst are illustrated in Fig. 15.

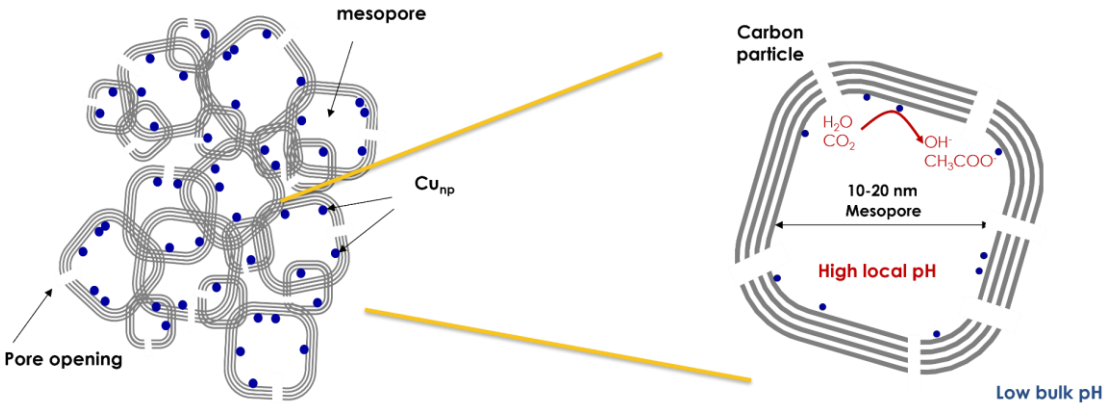

***Figure 15**: Structure and proposed working mechanism of the novel copper-based catalyst*

2.2.1 Synthesis of the catalyst

As the copper precursor, we used copper(II) nitrate hemi-pentahydrate ($Cu_2H_{10}N_4O_{17}$), a hydrated form of copper nitrate containing 2.5 molecules of water per formula unit. This compound typically appears as a light blue to turquoise crystalline solid, characteristic of Cu^{2+} ions. For the carbon support, we selected FCX650SE, a high-surface-area carbon material provided by Cabot Corporation. The new catalyst now on will be called as CuIN@FCX650SE. The synthesis began by dissolving the copper precursor in 20 mL of acetone using magnetic stirring. The carbon support was then added to the solution, followed by the addition of 20 mL of DIW. The resulting mixture was stirred for 20 minutes and then sonicated for an additional 20 minutes using a Fisher Brand CPX5800 ultrasonic bath to ensure proper dispersion. After sonication, the suspension was placed in a chemical oven and dried completely, yielding the initial composite, referred to as the "mother" material of the catalyst.

The final step involved a thermal reduction treatment in a Lindberg/Blue M Mini-Mite tube furnace (Thermo Fisher Scientific). The dried composite was heated to 300 °C for 2 hours under a reducing atmosphere composed of 5% H_2 and 95% Ar. This process effectively reduced copper oxide species to metallic copper [Cu(0)], forming the active catalyst.

A summary of the full catalyst preparation procedure is shown in Fig. 16.

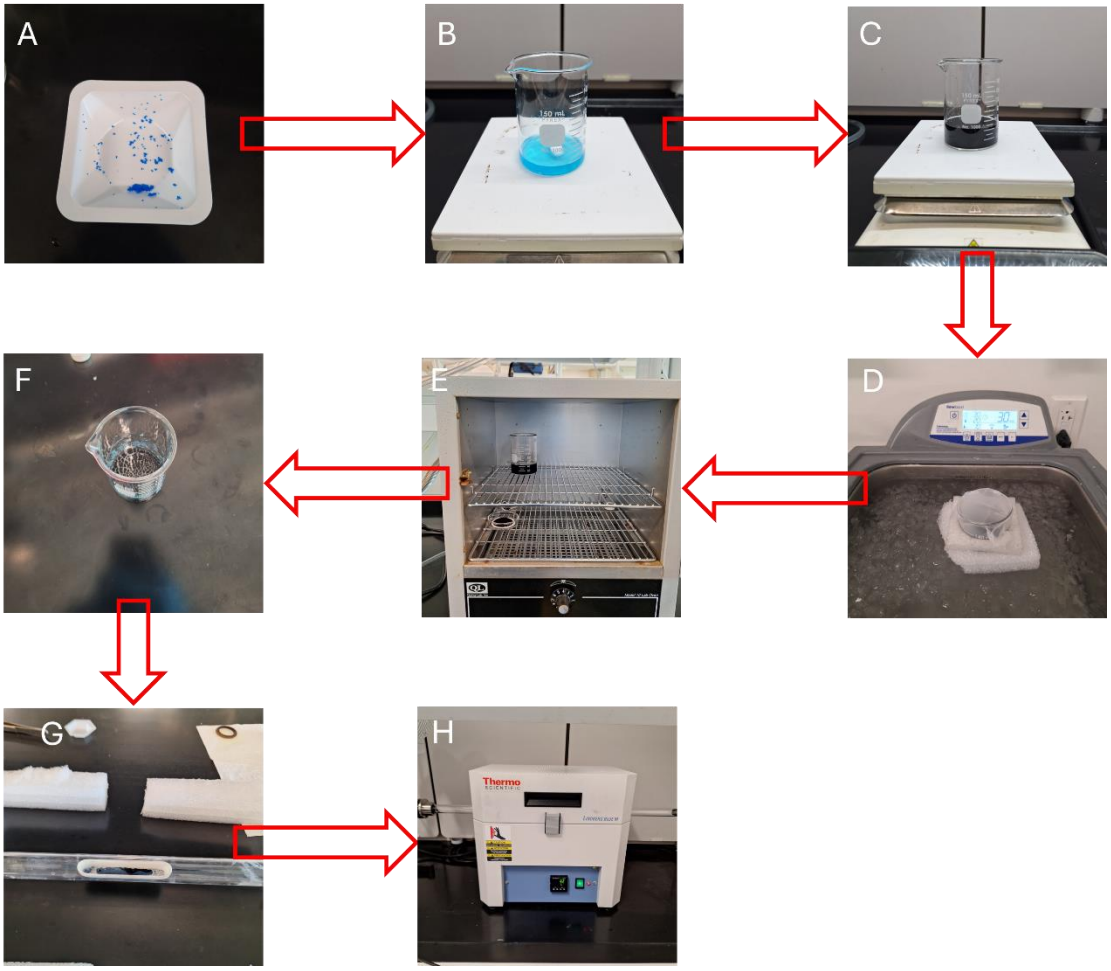

***Figure 16**: Procedure to make CuIN@FCX650SE. A) Weigh Copper Nitrate Hemi-Pentahydrate; B) Dissolve the copper precursor in acetone; C) Add the FCX650SE and stir for 20 minutes; D) Sonicate for 20 min E) Dry in the chemical oven; F) Put the catalyst in a boat; H) Heat treatment in the furnace*

2.2.2 Quantification of the final copper loading

To quantify the final copper loading (wt%) in our catalyst, we used a UV-Vis spectrophotometric method. The measurements were performed using a standard UV-Vis spectrophotometer (UV 2600 from Shimadzu), which operates by passing ultraviolet and visible light through a solution and measuring the absorbance at specific wavelengths. The absorbance is directly related to the concentration of the analyte in solution, according to the Lambert-Beer law, which states:

$$A = \varepsilon \cdot C \cdot l \qquad (2)$$

where A is the measured absorbance (unitless), ε is the molar absorptivity coefficient ($L \cdot mol^{-1} \cdot cm^{-1}$), C is the concentration of the absorbing species ($mol \cdot L^{-1}$), and l is the path length of the cuvette (usually 1 cm). This relationship allows us to calculate the concentration of a substance in solution, provided that ε and l are known.

Before the copper content could be analyzed, the carbon in the catalyst had to be completely removed. This was done by subjecting the sample to a thermal treatment at 850 °C for approximately 40 minutes, which ensured complete combustion of the carbon and left behind copper oxide (CuO). The resulting CuO was then dissolved in concentrated hydrochloric acid (38–40%), forming copper(II) chloride ($CuCl_2$).

To prepare the solution for UV-Vis analysis, the $CuCl_2$ solution was evaporated to dryness on a hot plate, and the resulting solid was re-dissolved in concentrated ammonium hydroxide (28–30%). In this medium, $CuCl_2$ forms a deep blue-colored complex whose concentration can be quantified by UV-Vis spectroscopy, since it shows a peak at a wavelength of 640 nm, as shown in Fig. 17.

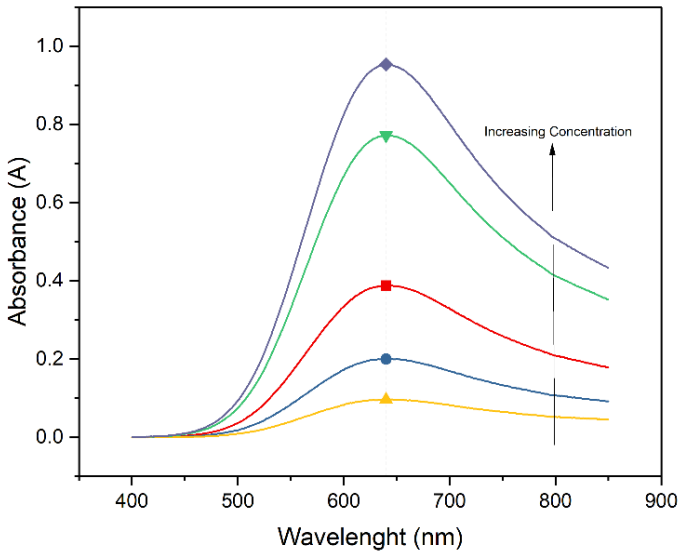

***Figure 17**: Uv-Vis Spectrum of CuCl2 in NH4OH*

To determine the copper concentration in our sample, we first constructed a calibration curve using known concentrations of $CuCl_2$. This calibration curve, shown in Fig. 18, relates absorbance at the characteristic peak wavelength to copper concentration. By measuring the absorbance of our unknown sample, we were able to determine its copper content using the standard curve and the Lambert-Beer law.

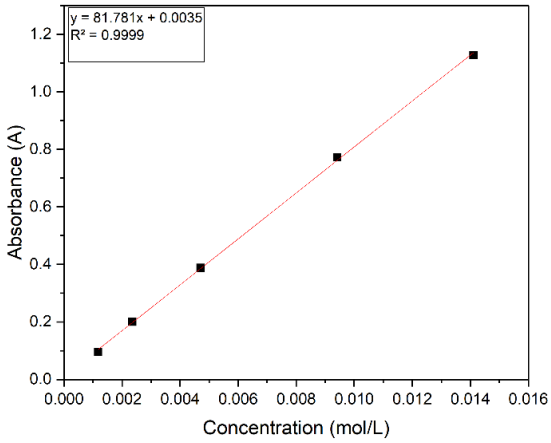

***Figure 18**: Calibration Curve to calculate the concentration of CuCl2*

2.3 Synthesis of Cu/Ag tandem catalyst

Once the new copper-based catalyst was synthesized, we tested its performance for both CO_2 and CO electroreduction in order to evaluate its catalytic behavior. The results from these experiments are discussed in more detail in Chapter 3. During these tests, we observed that the catalyst was able to produce Acetate during CO reduction, but not when using CO_2 as the feedstock. Based on this observation, we decided to couple the CuIN@FCX650SE catalyst with commercial silver nanoparticles, which are known for their high selectivity in converting CO_2 to CO. This tandem configuration was aimed at promoting a two-step cascade reaction, where CO_2 is first reduced to CO on silver, and then further reduced to Acetate on the copper nanoparticles.

In fact, Ag is one of the most efficient and selective catalysts for the electrochemical reduction of carbon dioxide to carbon monoxide. The reaction is a two-electron transfer process that converts CO_2 into CO with high Faradaic efficiency, often exceeding 90%, especially under neutral to slightly alkaline conditions. Silver is particularly attractive because it binds the *CO intermediate weakly enough to allow for its easy desorption, while still facilitating the activation of CO_2. This makes Ag an ideal first-step catalyst in tandem systems, where CO is subsequently used as a reactant for further reduction on a second catalyst, such as copper. Moreover, the low overpotential required for CO formation on Ag helps maintain energy efficiency in the overall electrochemical process [37].

To synthesize this new catalyst, we simply combined silver nanoparticles with our existing copper-based material. The idea was to obtain a final catalyst containing equal amounts of copper and silver by weight; so, knowing the copper content in CuIN@FCX650SE, we weighed out the same amount of silver nanoparticles.
We then mixed both components in 20 mL of acetone and left the mixture stirring overnight using a magnetic stir bar. The following day, we washed the resulting material three times with isopropanol. Each time, the catalyst was dispersed in the solvent, centrifuged for 5 minutes at 5000 rpm, and then the supernatant was discarded. This washing step was important not only to let the silver nanoparticles anchor onto the carbon structure, but also to help remove the polyvinylpyrrolidone (PVP) used as a surfactant to stabilize them.

After the final wash, the material was once again dispersed in isopropanol and filtered under vacuum to remove any remaining solvent. The catalyst was then left to dry overnight in a chemical oven. The entire synthesis process is outlined in Fig. 19. The new catalyst will be now on referred as Cu/Ag@FCX650SE.

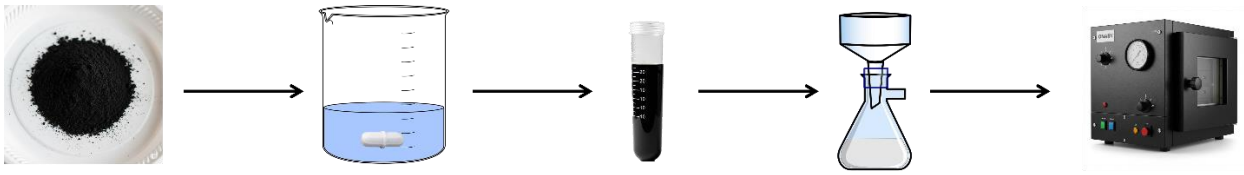

***Figure 19**: Procedure to obtain the Cu/Ag tandem catalyst*

With the same procedure, we obtained also another catalyst, just putting silver nanoparticles on the carbon support FCX650SE, this other catalyst will be referred as Ag@FCX650SE.

2.4 Characterization of the catalyst

To characterize the catalyst, we primarily used two techniques: X-ray diffraction (XRD) and transmission electron microscopy (TEM). The basic working principles of each method are briefly described in the following paragraphs.

2.4.1 X-ray diffraction

X-ray diffraction is a powerful technique used to investigate the crystallographic structure, phase composition, and average crystallite size of materials. When a crystalline sample is irradiated with X-rays, the atoms within the crystal lattice cause the incident X-rays to diffract at specific angles. These diffraction patterns follow Bragg's Law:

$$n\lambda = 2d\sin(\theta) \qquad (3)$$

which relates the wavelength of the X-rays (λ), the interplanar spacing (d), and the diffraction angle (θ). By analyzing the resulting diffraction peaks, one can identify the crystalline phases present and estimate crystallite size using the Scherrer equation. In our work, XRD was used to confirm the formation of metallic copper after the thermal reduction process and to assess the degree of crystallinity in the final catalyst [38].

2.4.2 Transmission Electron Microscopy

Transmission electron microscopy allows for the direct visualization of materials at the nanometer and even sub-nanometer scale. In this technique, a high-energy electron beam (typically 100–300 keV) is transmitted through an ultra-thin sample. As the electrons interact with the atoms in the sample, they produce contrast based on atomic number, density, and thickness, revealing detailed structural and morphological information. TEM can provide insights into particle size, shape, distribution, and even crystallographic orientation through

selected area electron diffraction (SAED). In this study, TEM was employed to characterize the morphology of the copper nanoparticles and their dispersion on the carbon support [39].

2.5 Electrochemical Setup and Testing Conditions

For the electrochemical tests, we used two types of electrolyzers: the H-Cell and the Flow Cell, both of which are described in detail in Sections 1.5.1 and 1.5.2. For the CO_2 reduction experiments, we employed both systems, since carbon dioxide has sufficiently high solubility in aqueous media, making it compatible with batch-type reactors like the H-Cell. On the other hand, the CO reduction tests were carried out exclusively using the Flow Cell, due to the low solubility of carbon monoxide in water, around 1.0 mM at 25 °C, which limits its effective use in closed systems such as the H-Cell.
The key electrochemical parameters and techniques applied in the various experiments will be summarized in the following sections.

2.5.1 Electrochemical Impedance Spectroscopy

Electrochemical Impedance Spectroscopy (EIS) is a technique used to study the interfacial properties of electrochemical systems. It works by applying a small alternating current (AC) voltage to an electrochemical cell over a range of frequencies and measuring the resulting current response. The ratio of voltage to current at each frequency gives the impedance, which reflects how easily electrons and ions move within the system. EIS can provide valuable information about various processes, such as charge transfer resistance, double-layer capacitance, mass transport limitations, and electrode/electrolyte interface behavior. The results are typically represented as Nyquist plots or Bode plots, which are then fitted to equivalent circuit models to extract meaningful physical parameters. Due to its sensitivity and non-destructive nature, EIS is widely used in catalyst evaluation, battery research, corrosion studies, and fuel cell development [40].

The resistance value obtained from this method was then used to perform iR compensation. This correction is crucial, because the potential applied to the working electrode includes not only the actual electrochemical potential at the interface between the catalyst and the electrolyte, but also the ohmic drop that occurs as current flows through the electrolyte. If we don't account for this resistance, the potential applied to the system will differ from the one we actually intend to apply, leading to inaccurate electrochemical data. The corrected potential can be calculated using the following formula:

$$E_{iR-Corrected} = E - i * R \quad (4)$$

Where $E_{iR\text{-}Corrected}$ is the actual potential applied to the system, E is the measured potential, i is the measured current and R is the ohmic resistance of the electrolyte. By applying this correction, we ensure that the electrochemical behavior observed is representative of the true performance of the catalyst, without distortion from resistive losses in the cell.

2.5.2 Cyclic Voltammetry

Cyclic Voltammetry (CV) is one of the most widely used electrochemical techniques for studying the redox behavior of materials and characterizing electrode surfaces. In a CV experiment, the potential of the working electrode is swept linearly with time, first in one direction and then reversed back, creating a triangular waveform. The resulting current is recorded as a function of the applied potential, generating a cyclic voltammogram, represented in Fig. 20.

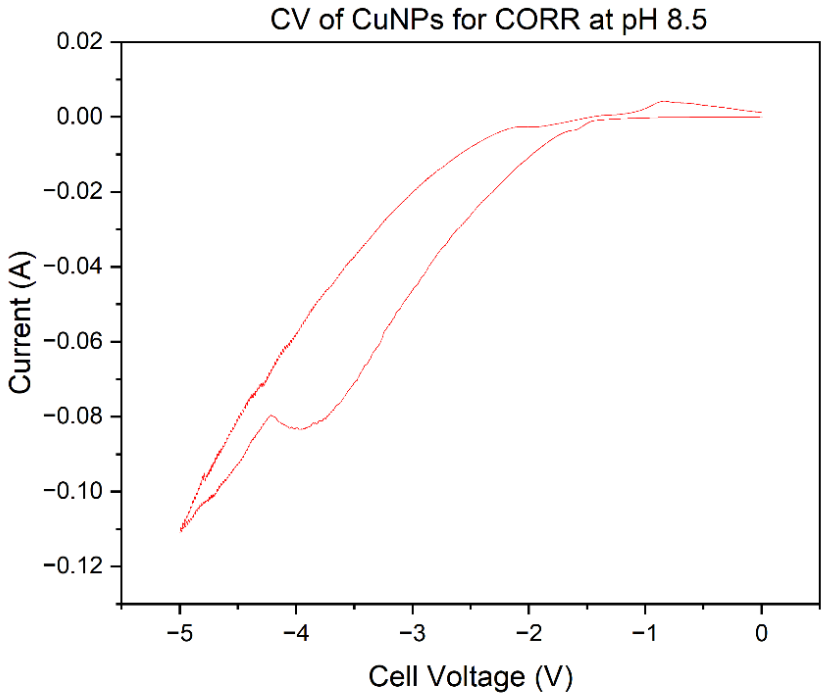

***Figure 20**: Example of the Cyclic Voltammetry for CuNPs in the flow cell*

The CV is used to see which current corresponds to a certain potential that we want to apply to the system and it is often used to see the activity of a certain catalyst.

2.5.3 Chronoamperometry

Chronoamperometry (CA) is a time-resolved electrochemical technique used to study the stability and catalytic performance of electrode materials under constant operating conditions. In a CA experiment, the potential of the working electrode is stepped to a fixed value and held constant while the resulting current is monitored over time. This allows us to observe how the system behaves under steady-state conditions, providing valuable information about catalytic activity, deactivation processes, and long-term stability.
In the context of CO_2 and CO electroreduction, CA is particularly useful for evaluating how the current evolves under a constant applied potential. A stable current over time generally indicates

that the catalyst maintains its activity, while a decaying current may signal deactivation, mass transport limitations, or surface poisoning by reaction intermediates.

An example of a CA registered during one of the experiments is represented in Fig. 21.

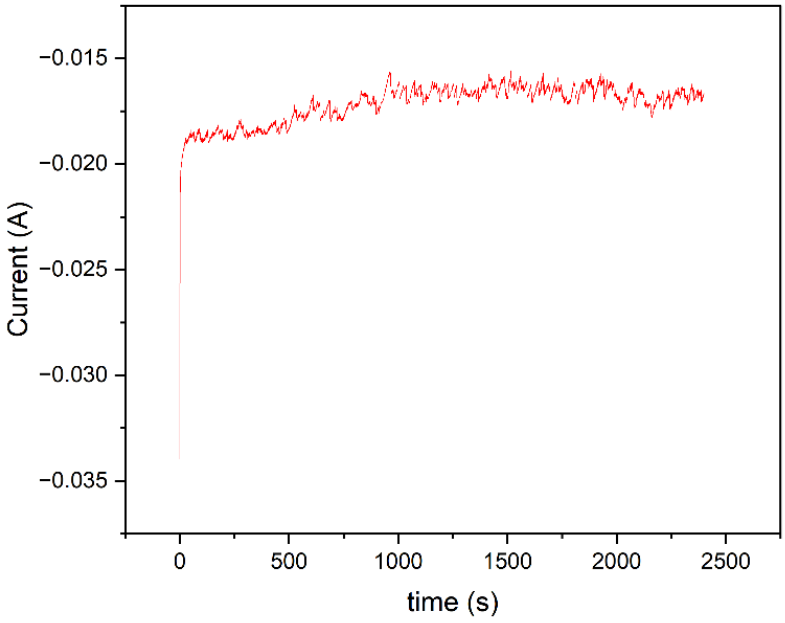

***Figure 21**: Example of a Chronoamperometry for CuNPs in the flow cell*

2.5.4 Faradaic Efficiency

Faradaic Efficiency (FE) is a key parameter used to evaluate the selectivity of an electrocatalyst during an electrochemical reaction. It represents the fraction of electrical charge that is effectively used to produce a specific chemical product, as opposed to being consumed in competing side reactions, such as hydrogen evolution reaction. FE is crucial when assessing the performance of catalysts for CO_2 or CO electroreduction, where multiple products can form simultaneously, each requiring different numbers of electrons.
The Faradaic efficiency for a given product *i* is calculated using the following formula (eq. 5):

$$FE_i = \frac{n_i * F * C_i * V}{Q_{total}} \quad (5)$$

Where n_i is the number of electrons required to produce one molecule of product *i*, *F* is Faraday's constant (96485 C/mol), C_i is the concentration of product *i* (in mol/L), *V* is the volume of the electrolyte (in L), Q_{total} is the total charge passed during the experiment (in C).

A high Faradaic efficiency indicates that most of the input electrical energy is being used to produce the desired product, making it a critical performance metric in the development of sustainable and efficient electrocatalytic systems.

2.5.5. Yield Rate

The yield rate is a measure of the total number of moles produced during a given electrochemical test, divided by the duration of the experiment and the active surface area of the catalyst used. It can be calculated using the following equation:

$$Y_i = \frac{N_i}{t*A} \quad (6)$$

Where N_i is the number of moles produced for a certain chemical species, t is the duration of the experiment and A is the active area of the catalyst.

2.6 Quantification of liquid products

To quantify the concentration of the liquid products that we produce during our experiments we used two types of techniques, ^{1}H-NMR and HPLC; in the following sections we are going to discuss briefly what are the main principles behind these analysis techniques.

2.6.1 ^{1}H-NMR Spectroscopy

^{1}H-NMR (Proton Nuclear Magnetic Resonance) spectroscopy is an analytical technique used to identify and quantify organic molecules by analyzing the magnetic environment of hydrogen atoms (protons) within a compound. The method is based on the fact that hydrogen nuclei have a magnetic moment and will align with or against an external magnetic field. When a radiofrequency (RF) pulse is applied, these nuclei absorb energy and transition between spin states. As they relax back to their original state, they emit a signal that is detected and translated into an NMR spectrum. The position (chemical shift) and shape of each signal provide detailed information about the chemical structure, functional groups, and proton environment within the molecule. In CO_2 and CO electroreduction studies, ^{1}H-NMR is commonly used to identify and quantify liquid-phase products such as Ethanol, Acetate, and Formate, often using internal standards to improve accuracy [41].

2.6.2 High Performance Liquid Chromatography (HPLC)

High Performance Liquid Chromatography (HPLC) is an essential analytical technique for separating, identifying, and quantifying components in liquid mixtures. The system consists of a high-pressure pump that pushes the liquid sample through a column packed with a stationary phase, typically composed of small particles. As the sample travels through the column, its components interact differently with the stationary phase depending on their polarity, size, or chemical affinity, causing them to separate. Each compound exits the column at a characteristic retention time and is detected using UV-Vis detectors or refractive index detectors. HPLC is widely used in electrochemical CO_2 reduction research to quantify small organic acids like formic acid and acetic acid, which may be difficult to distinguish by other techniques. It offers

high sensitivity, reproducibility, and the ability to analyze non-volatile or thermally unstable species [42].

2.7 Experimental tests

2.7.1 Experimental tests in the H-Cell

Initial tests on copper-based catalysts for the electrochemical reduction of CO_2, including commercial copper nanoparticles (CuNPs) and CuNPs supported on NiNC, were carried out using an H-Cell configuration.

To test the various catalysts, they were first dispersed in a solvent mixture to prepare an ink, which was then drop-cast onto a carbon paper with an active geometric area of 1 cm^2. The ink formulation used was as follows: 5 mg of catalyst, 670 µL of isopropanol (IPA), 300 µL of deionized water (DIW), and 30 µL of Nafion solution. A total of 100 µL of ink was deposited per electrode, corresponding to a loading of 0.5 mg/cm^2 of catalyst.

The electrolyte used for these experiments was 0.2 M potassium bicarbonate ($KHCO_3$).

The testing protocol included an initial EIS measurement to determine the system resistance, followed by CV to assess the electrochemical activity of the catalyst. Then, CA was performed at constant potentials ranging from –0.6 V to –1.0 V vs. RHE, with each test lasting one hour. An iR compensation was applied, correcting for 85% of the measured resistance.

After each CA test, the catholyte was collected and replaced with fresh electrolyte. The collected samples were analyzed using ^{1}H-NMR spectroscopy to identify and quantify the liquid-phase products.

However, the current densities obtained in the H-cell setup were relatively low, and Formate ($HCOO^-$) was the only product detected by NMR. Due to these limitations, the focus shifted to using a flow cell system, which allows for higher current densities. Additionally, HPLC was employed for product quantification, given its lower detection limits and greater sensitivity compared to NMR.

2.7.2 Experimental tests in the Flow Cell

In the flow cell setup, all synthesized and commercial catalysts were tested for both CO_2 reduction and CO reduction. The catalysts studied include commercial CuNPs, as well as the newly synthesized CuIN@FCX650SE, Ag@FCX650SE, Cu/Ag@FCX650SE.

As electrochemical measurements, we performed an initial CV and then we did a CA between -3V and -5V as cell voltage. In a flow cell configuration, the applied potential is typically reported as the overall cell voltage, rather than referenced to a standard electrode such as RHE. This is because most flow cell systems are designed as membrane-separated, two-electrode configurations, where the focus is on the total voltage required to drive the full electrochemical reaction from cathode to anode.

For these experiments, the ink was prepared using the following recipe: 25 mg of catalyst, 3 mL of isopropanol (IPA), and 20 µL of Nafion solution. A volume of 360 µL of this ink was deposited onto a gas diffusion electrode (GDE), covering an area of 3 cm^2, which corresponds to a nominal loading of 1 mg/cm^2. However, the active geometric area exposed to the electrolyte in the flow cell was only 1 cm^2. In the case of CuIN@FCX650SE, 540 µL of ink was used to increase the number of accessible active sites for catalysis.

The first catalyst tested in the flow cell was commercial CuNPs. These were initially used to perform a pH screening experiment for the electrochemical reduction of CO, aimed at evaluating the role of pH in the system. The pH was varied between 8.5 and 13.5, using six distinct values. This was achieved by mixing 0.2 M $KHCO_3$ (pH 8.5) and 1 M KOH (pH 13.5) solutions in different proportions. After this study, the same CuNPs catalyst was also tested for CO_2 reduction, using 0.2 M $KHCO_3$ as the electrolyte.

The second catalyst tested was the newly developed CuIN@FCX650SE. This catalyst was evaluated at pH 8.5 (0.2 M $KHCO_3$), because it is the pH that we use for CO2RR . It was also tested for CO_2RR in 0.2 M $KHCO_3$ electrolyte to assess its performance in CO_2 reduction at neutral pH.

Finally, we tested also Ag@FCX650SE and Cu/Ag@FCX650SE for CO_2 reduction, using 0.2M $KHCO_3$ as electrolyte.

3. Results

3.1 Characterization of the new catalysts

In this paragraph we are going to discuss the main results of the characterization of the new catalysts through XRD and TEM analysis.

3.1.1 Characterization of CuIN@FCX650SE

In the synthesis of the novel copper catalyst CuIN@FCX650SE we aimed first to obtain a catalyst with 30 wt% of copper following the procedure illustrated in Fig. 16, but the copper loading was too high and so the copper particles formed big aggregates and didn't attach to the carbon surface, as we can see in Fig. 22.

***Figure 22**: CuIN@FCX650SE with 30% copper loading*

Because of this, we reduced the amount of copper inside our catalyst, and we made two different tests with a copper loading of 10 wt% and 15 wt%. We quantified also the final copper loading in these two catalysts through the method shown in the chapter 2.2.2, obtaining a final weight percentage of 5.44% for the 10 wt% loading and 13.41% for the 15 wt% loading. So, we decided to use the 15 wt% loading catalyst for our tests.

We analyzed the samples of the two catalysts with the different loadings with the TEM, so we can compare and see the differences between the two on the nanoscale. In Fig. 23, we can get a general overview of the nanoscale structure of our catalyst. On the left, we see the sample with 10 wt% copper loading, while on the right there is the one with 15 wt%. The dark spots represent the copper particles embedded within the carbon structure. As observed, the catalyst with 10 wt% copper contains only a small number of dispersed copper particles inside the FCX650SE matrix, which is also confirmed by the UV-Vis quantification. The distribution appears uneven, likely due to the limited amount of metal present. On the other hand, in the catalyst with 15 wt% copper, the copper particles are much more uniformly distributed throughout the carbon structure, although their particle sizes vary.

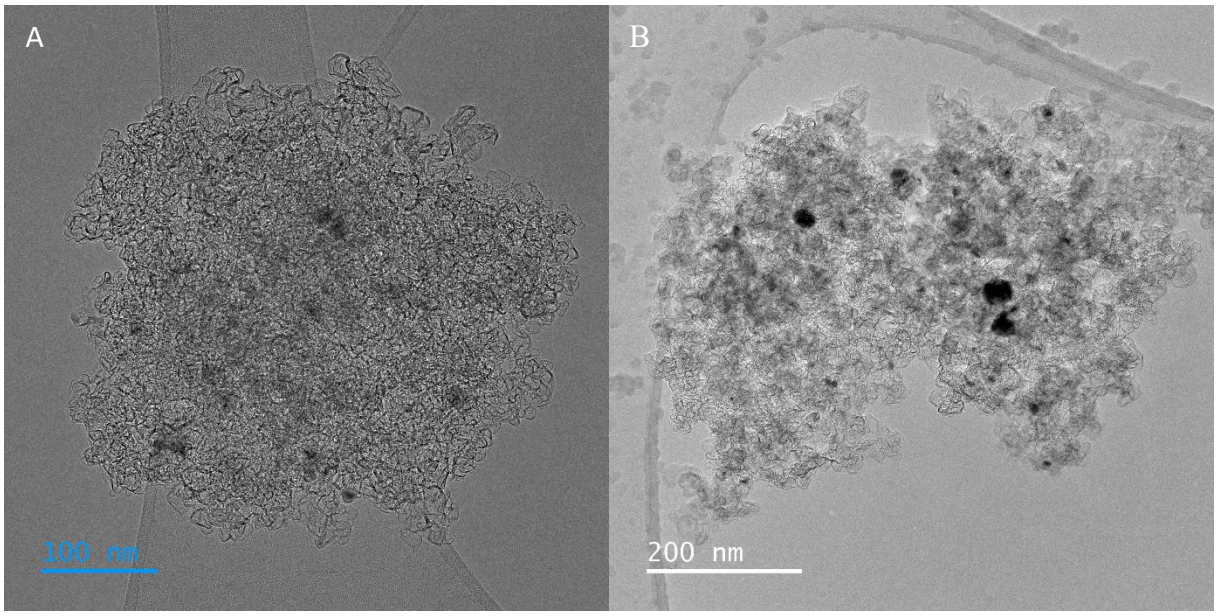

***Figure 23**: Overall TEM image of CuIN@FCX650SE with 10 wt% (A) and 15 wt% (B) copper loading*

By zooming in, we can take a closer look at the shape and distribution of the copper nanoparticles. In Fig. 24A, a portion of the carbon structure is shown in detail, where the particles appear to be fairly evenly distributed. In Fig. 24B, we can observe both the morphology and the variation in particle size more clearly. Despite this variation, the larger particles measure around 30 nm, which is comparable to the size of the commercial copper nanoparticles used during the pH screening experiments.

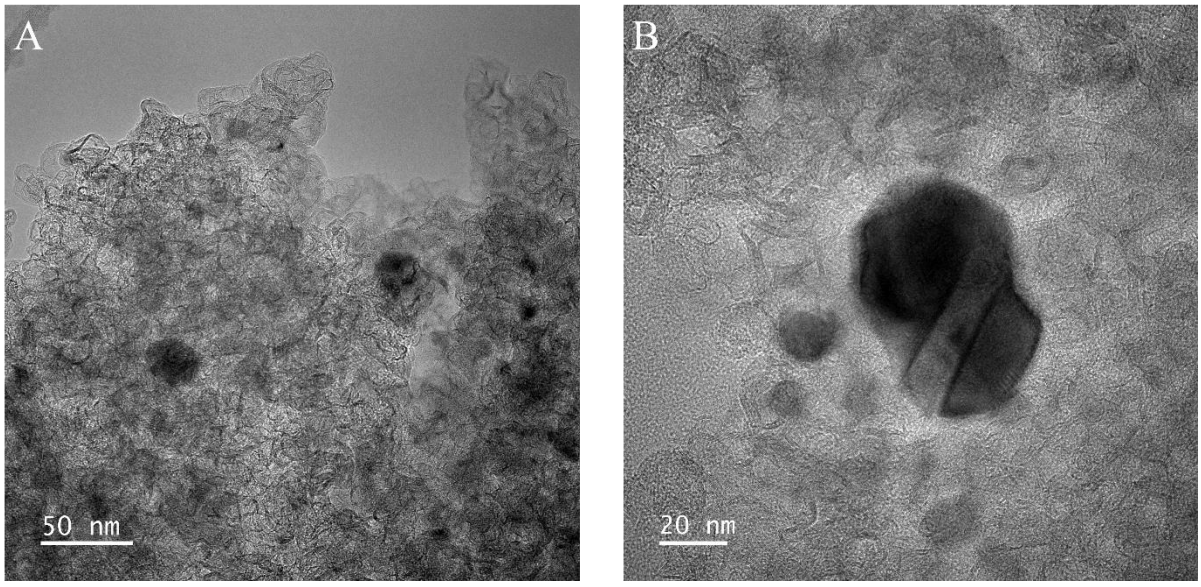

***Figure 24**A: Zoom of a portion of the catalyst structure; 24B: Morphology and particle size of copper nanoparticles*

To determine which crystalline phases are present in our catalyst, we performed an XRD analysis and compared the results with data reported in the literature (Fig. 25). The main crystalline phases identified for copper are Cu (111), Cu (200), and Cu (220), although the latter is not shown in the figure [43]. From the XRD pattern, it is evident that the catalyst with 15 wt% copper loading contains a significantly higher amount of copper compared to the one with 10 wt%.

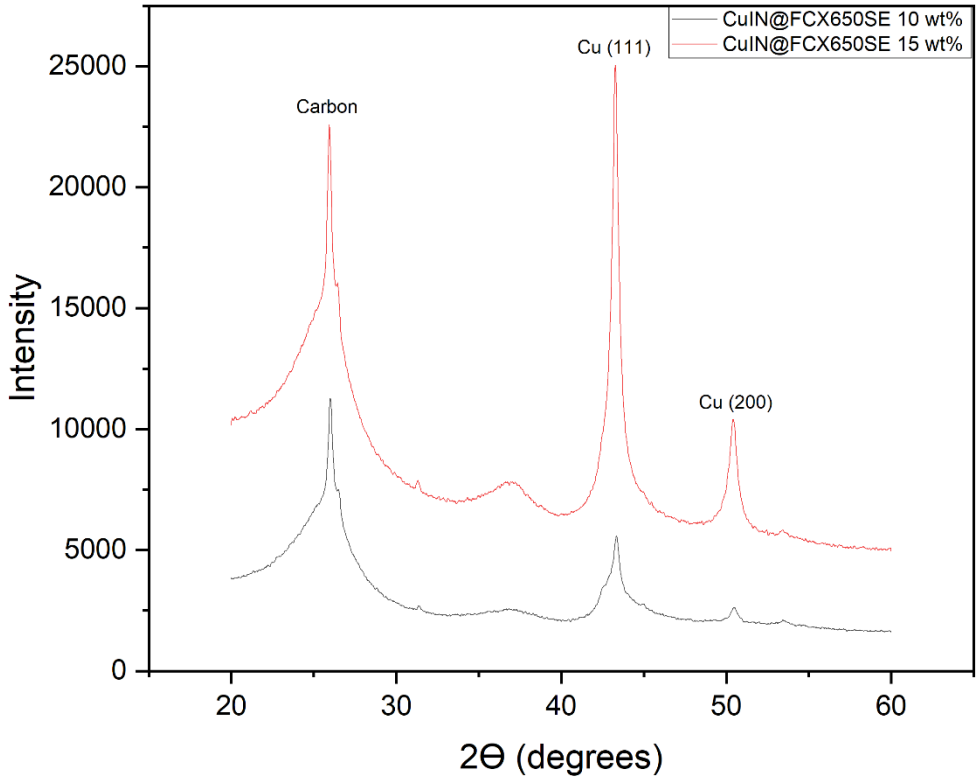

***Figure 25**: XRD pattern of CuIN@FCX650SE with 10 wt% and 15 wt% copper loading*

3.1.2 Characterization of Cu/Ag@FCX650SE

For the catalyst containing both silver and copper nanoparticles, we weighed 100 mg of the previously synthesized copper-based material, which contained 13.41 mg of copper, and mixed it with an equal amount of commercial silver nanoparticles. As a result, we obtained a final catalyst containing 11.82 wt% of both copper and silver.

The same procedure described in the latter paragraph has been repeated to characterize also the catalyst with copper and silver nanoparticles.

Through XRD analysis of the newly synthesized catalyst, we were able to identify the different crystalline phases present in the sample. By comparing the diffraction peaks with reference data from the literature for both silver and copper nanoparticles, we confirmed the presence of both metals in the material [43,44]. The XRD pattern of the Cu/Ag@FCX650SE catalyst is shown in Fig. 26.

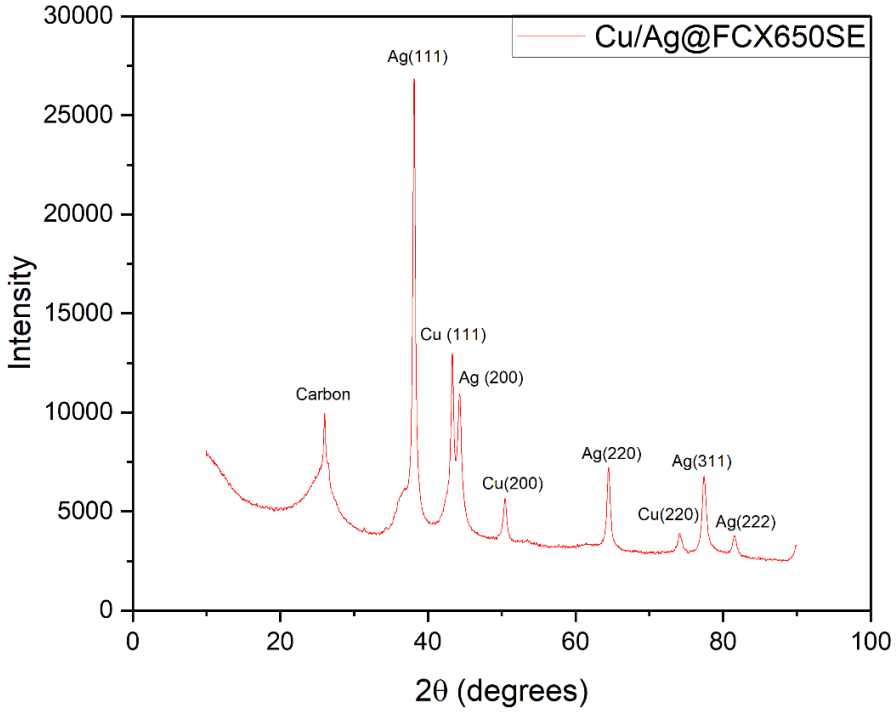

***Figure 26**: XRD pattern of Cu/Ag@FCX650SE*

We then analyzed the new material using transmission electron microscopy to observe the coexistence and size of the two metallic components. In Fig. 27A, we can see a general overview of the sample, where the commercial silver nanoparticles, which have a nominal size of around 100 nanometers, are clearly visible. In Fig. 27B, the coexistence of both types of nanoparticles becomes more apparent. The silver nanoparticles are located on top of the carbon structure, while the smaller copper nanoparticles are able to embed themselves in the gaps between the graphitic layers of the FCX650SE carbon support.

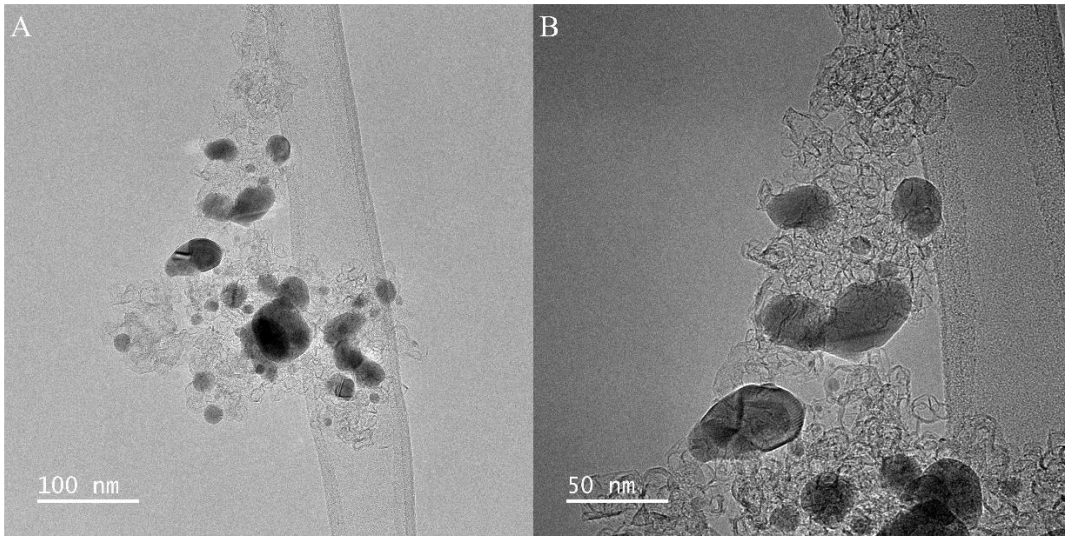

***Figure 27** A: Overall TEM image of Cu/Ag@FCX650SE, 27B: Copper and silver nanoparticles in a portion of the carbon structure*

3.2 pH screening with CO reduction

The pH screening was carried out for the CORR to determine under which pH and voltage conditions we obtain the highest production of Acetate and other products. To describe the results, we calculated both the Faradaic efficiency and the yield rate, and the outcomes are summarized in the following graphs.

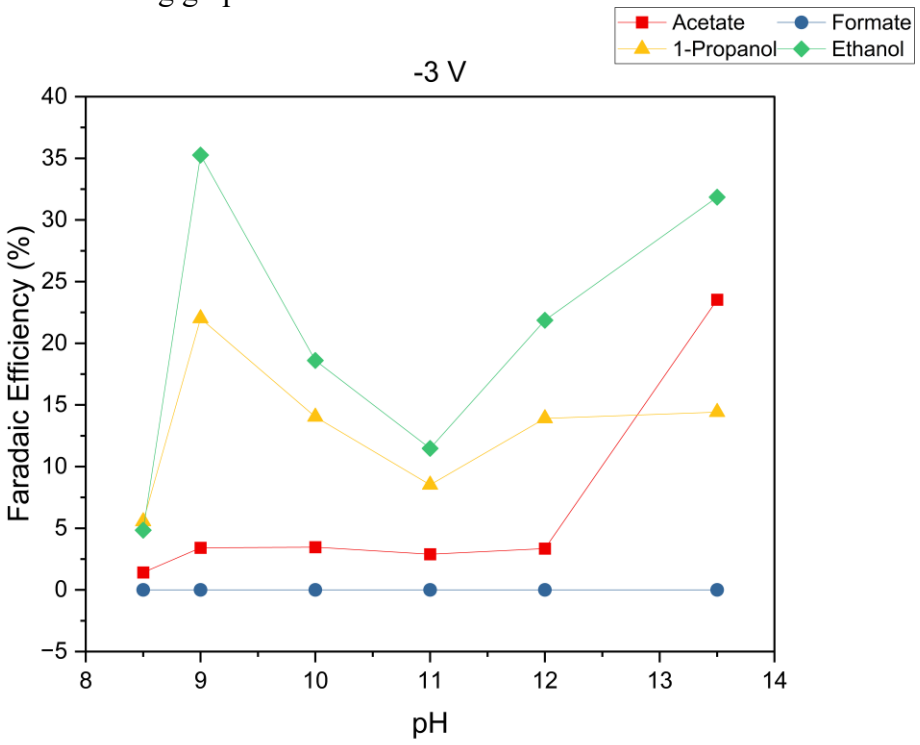

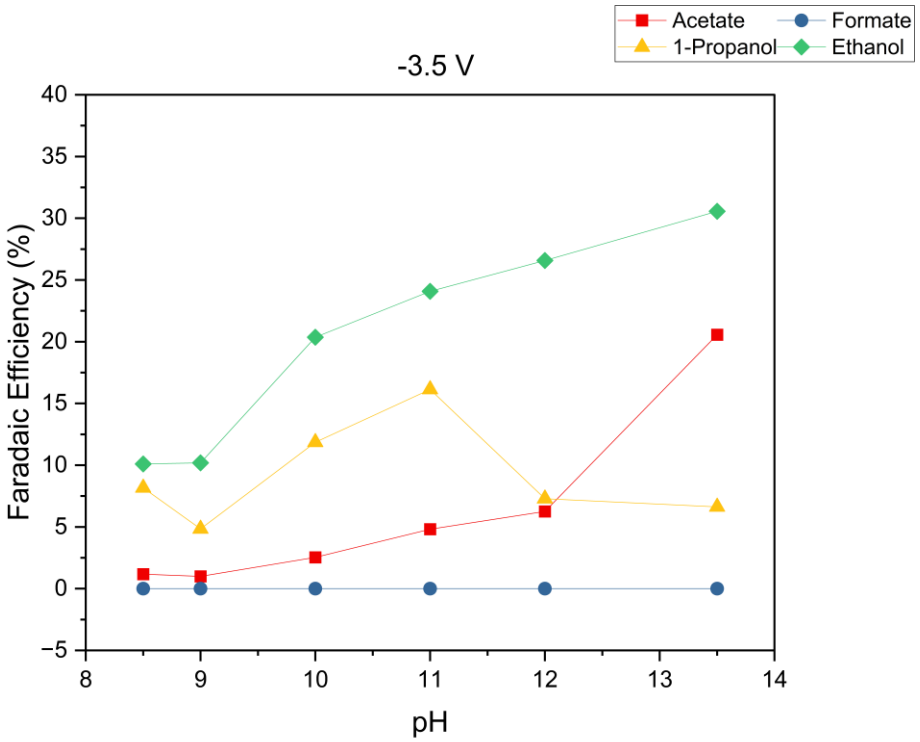

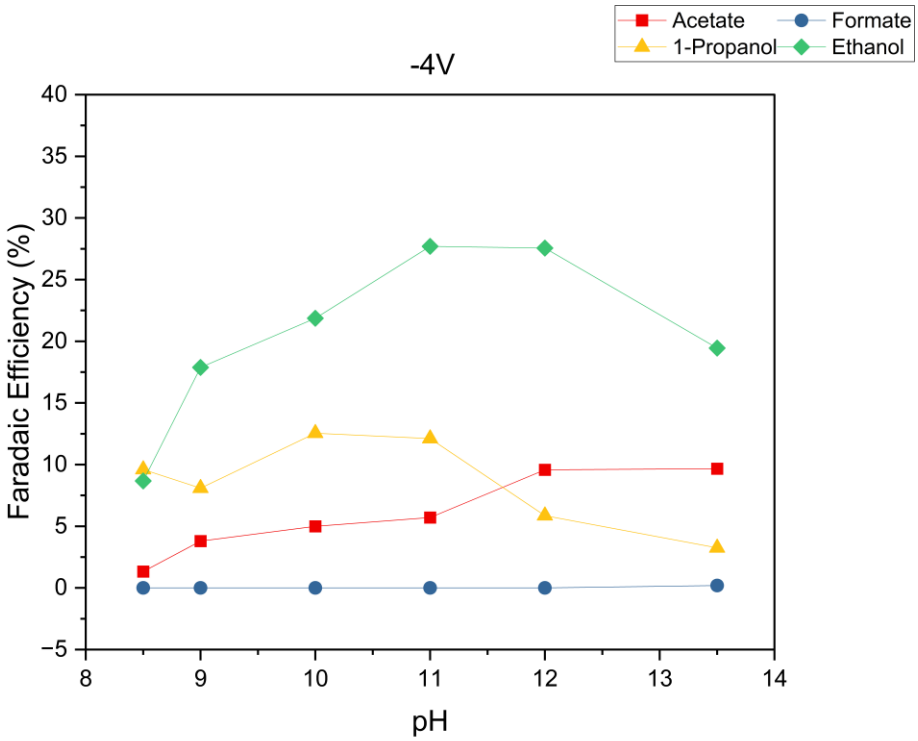
Acetate
Formate
1-Propanol
Ethanol
-4V
Faradaic Efficiency (%)
pH
40
35
30
25
20
15
10
5
0
−5
8
9
10
11
12
13
14

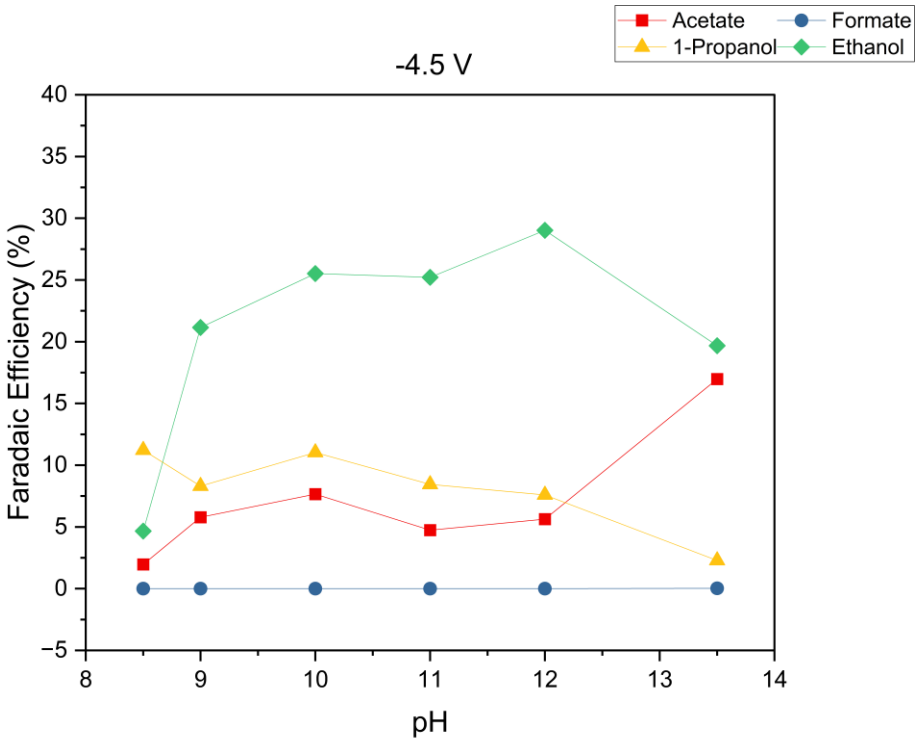
Acetate
Formate
1-Propanol
Ethanol
-4.5 V
Faradaic Efficiency (%)
pH
40
35
30
25
20
15
10
5
0
−5
8
9
10
11
12
13
14

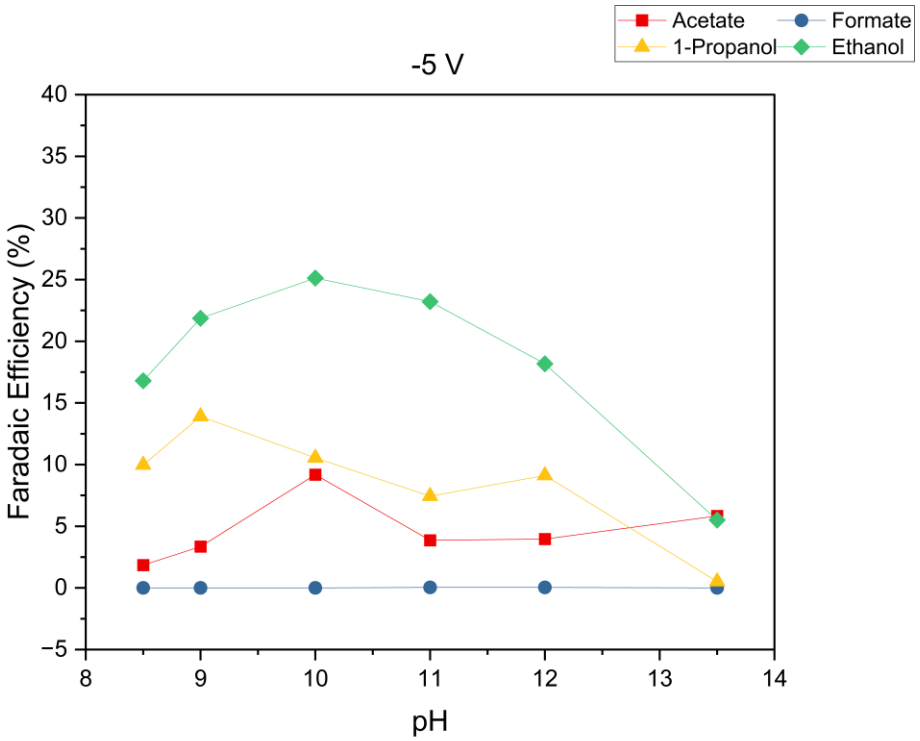

***Figure 28**: Trend of the faradaic efficiencies for Acetate, 1-Propanol, Ethanol and Formate varying the pH at different potentials*

From Fig. 28, we can observe the trend of the Faradaic efficiencies of the main CORR products as a function of pH at the different cell voltage values applied. Regarding Acetate, which is the product of our interest, it can be noted that the Faradaic efficiency reaches its maximum when using 1 M KOH solution (pH 13.5) for almost all the cell voltage values tested, except for −5 V. At this cell voltage, however, the Faradaic efficiency of Acetate is generally quite low, and there is a high production of gaseous products, as can be better seen in Fig. 29. In particular, the highest calculated Faradaic efficiency was obtained at a voltage of −3 V and with a pH of 13.5, reaching 23.54%. As for the other products, the Faradaic efficiency for Formate is almost always equal to zero; this is because, starting from CO instead of CO_2, we cannot obtain the necessary reaction intermediate for its formation, as illustrated in the mechanism in Fig. 4. Finally, for Ethanol and 1-Propanol, no clear trend is observed with respect to pH variation, and their production is strongly dependent on the applied voltage.

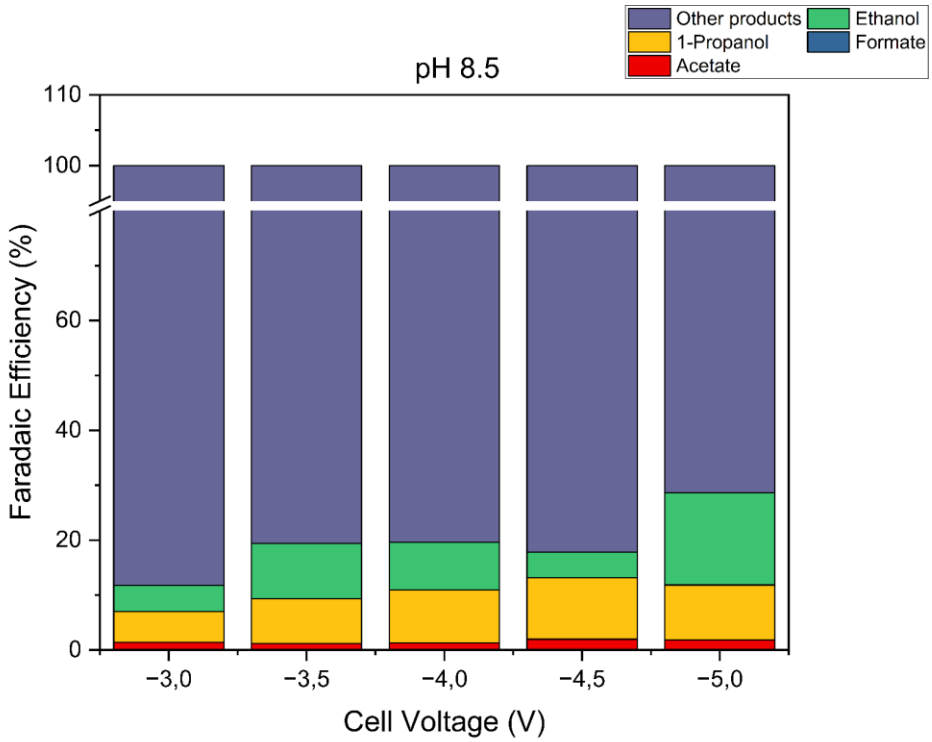
pH 8.5
Other products
Ethanol
1-Propanol
Formate
Acetate
Faradaic Efficiency (%)
110
100
60
40
20
0
−3,0
−3,5
−4,0
−4,5
−5,0
Cell Voltage (V)

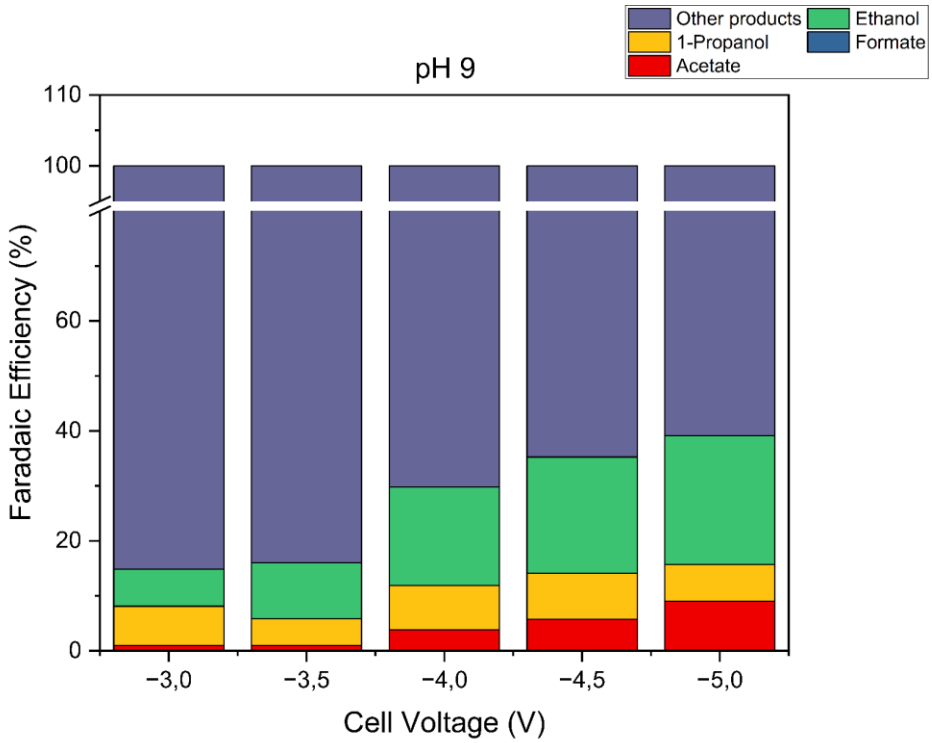
pH 9
Other products
Ethanol
1-Propanol
Formate
Acetate
Faradaic Efficiency (%)
110
100
60
40
20
0
−3,0
−3,5
−4,0
−4,5
−5,0
Cell Voltage (V)

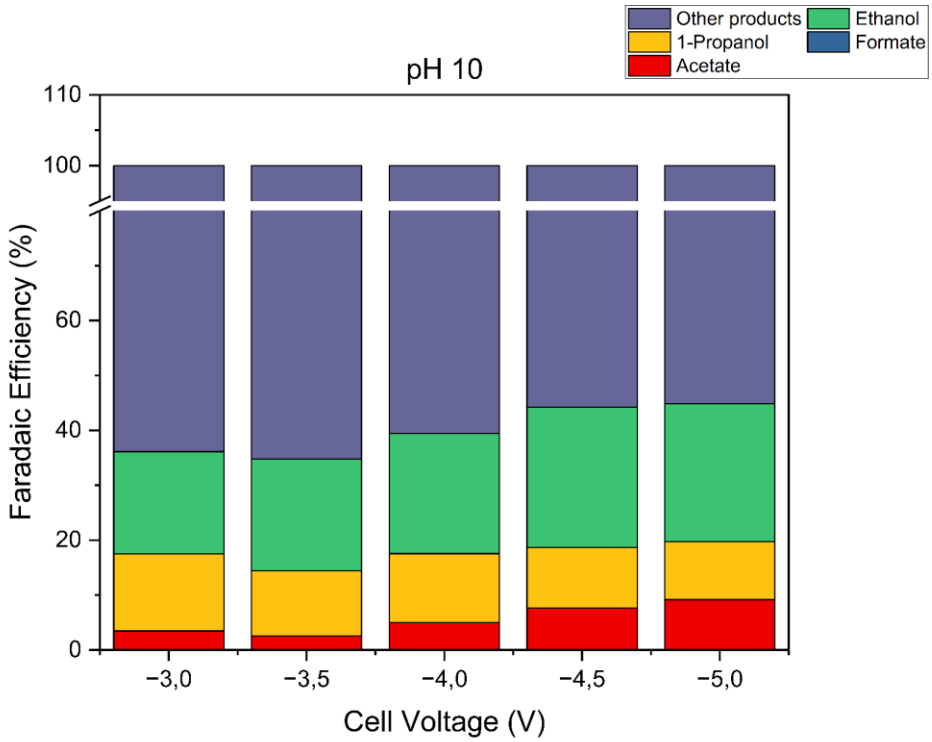
pH 10
Other products
Ethanol
1-Propanol
Formate
Acetate
Faradaic Efficiency (%)
110
100
60
40
20
0
−3,0
−3,5
−4,0
−4,5
−5,0
Cell Voltage (V)

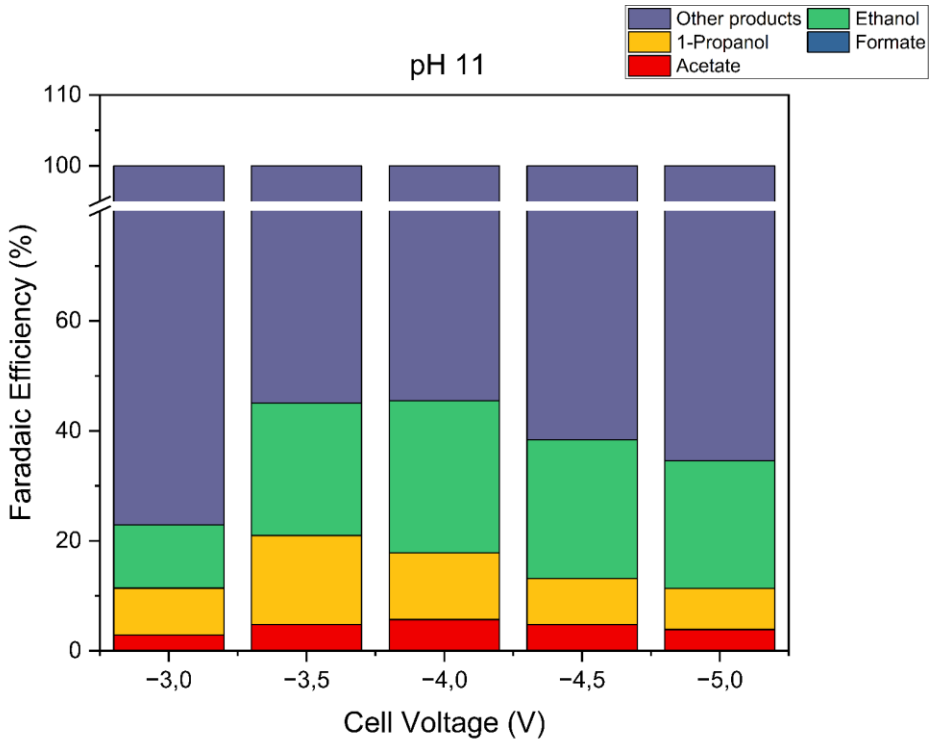
pH 11
Other products
Ethanol
1-Propanol
Formate
Acetate
Faradaic Efficiency (%)
110
100
60
40
20
0
−3,0
−3,5
−4,0
−4,5
−5,0
Cell Voltage (V)

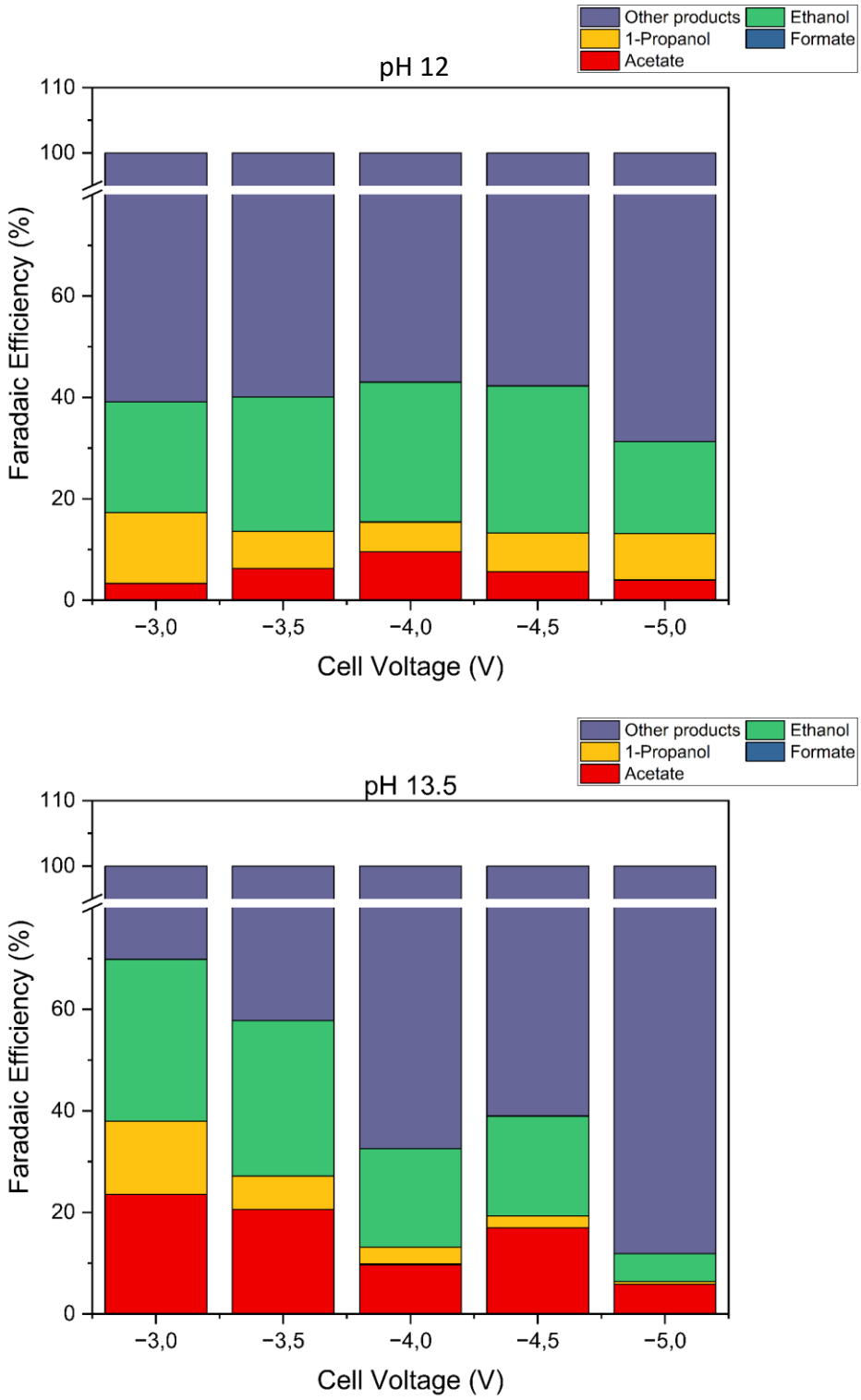

***Figure 29**: Bar charts of the Faradaic efficiencies for the liquid products varying the cell voltage, at different pH*

To better understand the overall Faradaic efficiency toward liquid products, we can analyze the graph in Fig. 29. It shows that, at practically all voltages, the main products are not liquids but rather gaseous species such as hydrogen, ethylene, and methane. In the legend, the term "other products" is reported, as these could also include other liquid products; however, their

concentration is too low to be detected through HPLC. Another point that emerges from these graphs is the clear difference in Faradaic efficiency toward Acetate at pH 13.5 compared to all the other pH values tested. Finally, the liquid product obtained with the highest Faradaic efficiency starting from carbon monoxide is, in almost all the cases analyzed, Ethanol.

Finally, from the graphs in Fig. 30, we can analyze the trend of the yield rate, which provides insight into the total number of moles produced for each liquid product. From these graphs, we can also observe that at a pH of 13.5, the number of moles produced for Acetate and Ethanol consistently reaches a clear maximum, highlighting that these conditions are the most favorable for their production. In the case of 1-Propanol, however, this trend was not observed; in fact, the yield rate remains fairly constant across all pH values.

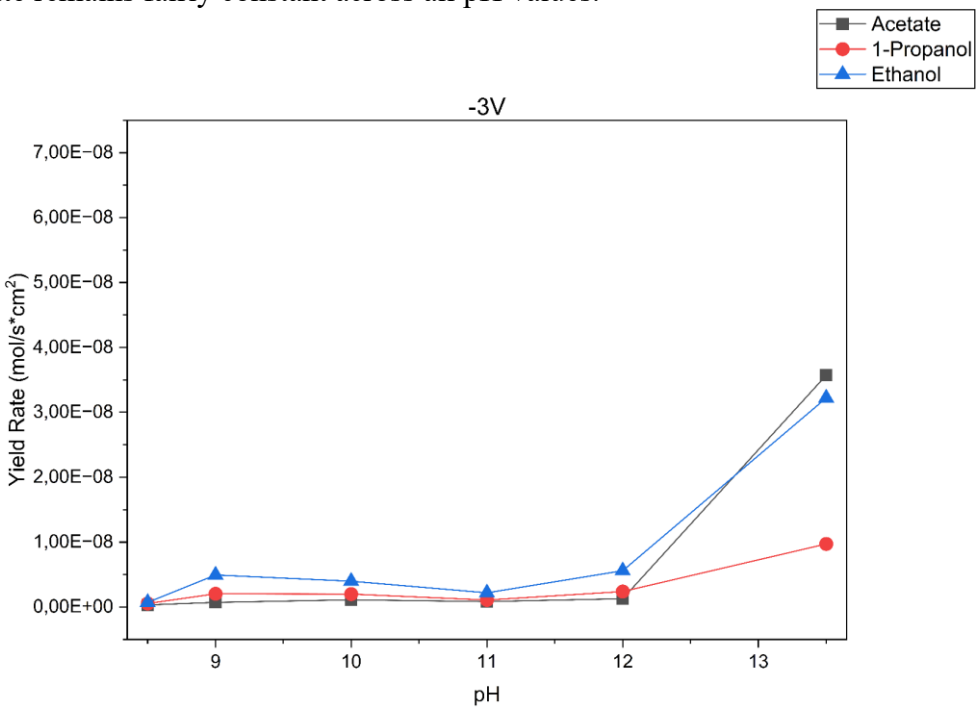

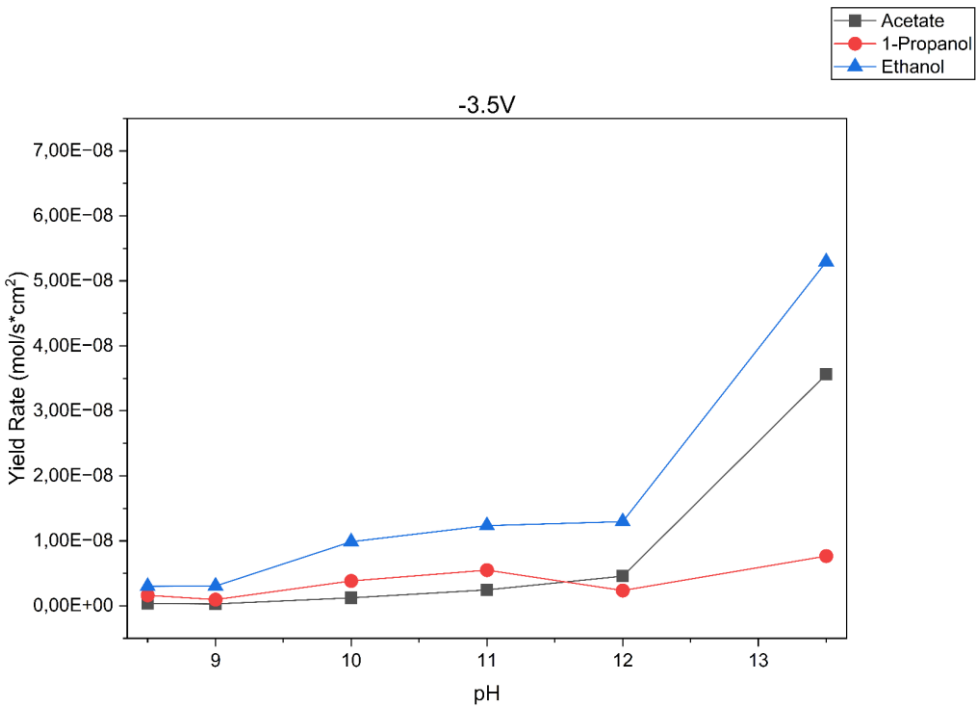

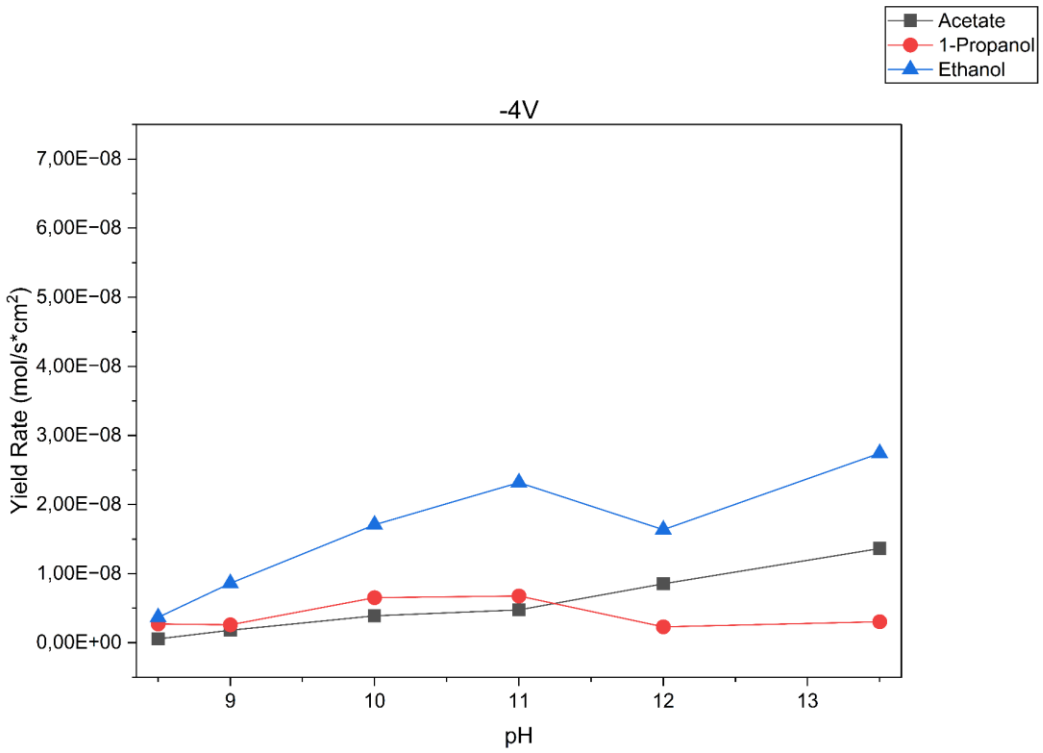
Acetate
1-Propanol
Ethanol
-4V
7,00E−08
6,00E−08
5,00E−08
4,00E−08
3,00E−08
2,00E−08
1,00E−08
0,00E+00
Yield Rate (mol/s*cm²)
9
10
11
12
13
pH

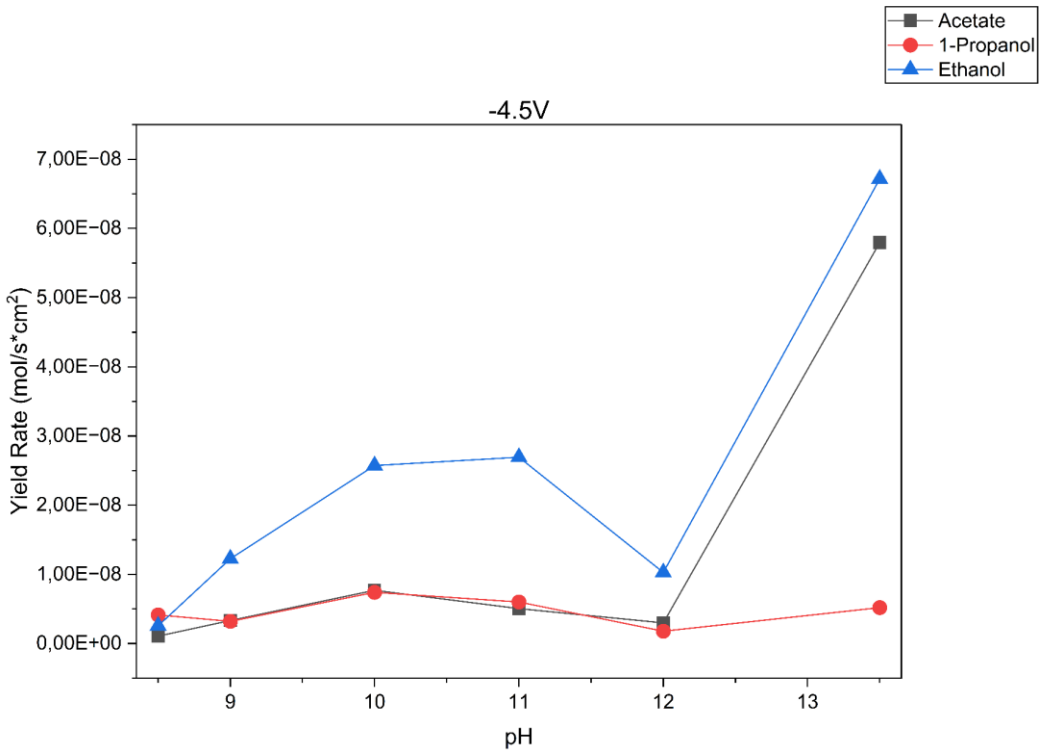
Acetate
1-Propanol
Ethanol
-4.5V
7,00E−08
6,00E−08
5,00E−08
4,00E−08
3,00E−08
2,00E−08
1,00E−08
0,00E+00
Yield Rate (mol/s*cm²)
9
10
11
12
13
pH

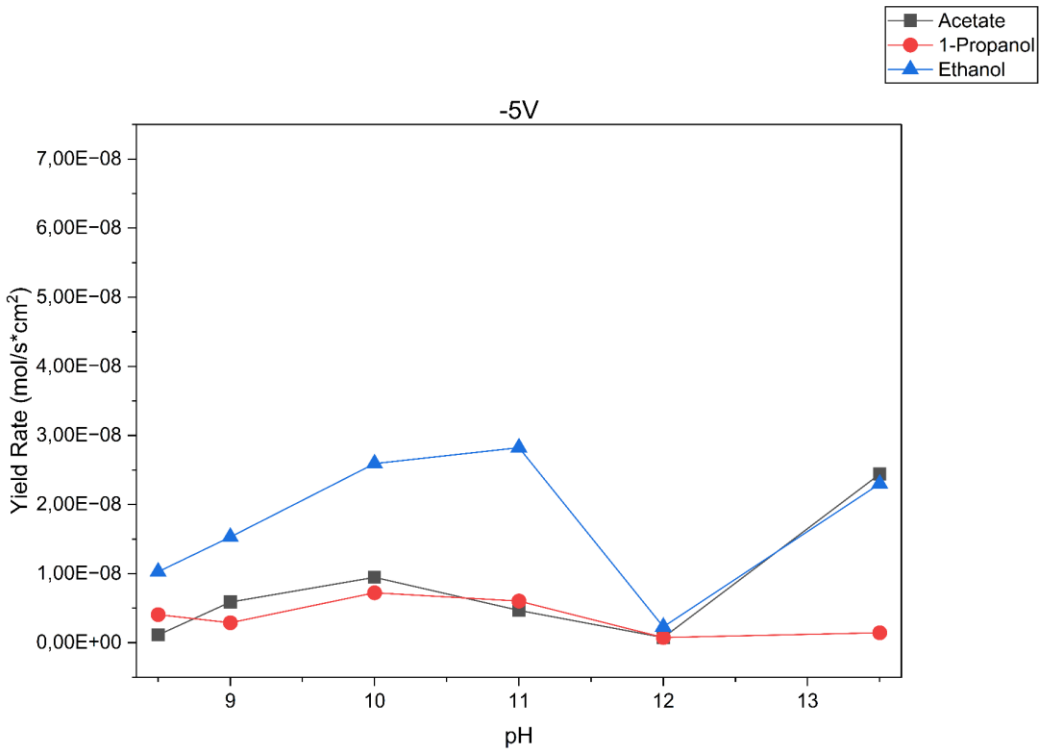

***Figure 30**: Yield rate of the liquid products varying the pH, at different cell voltages*

In conclusion, from this pH screening we confirmed that the optimal conditions for Acetate production are at high pH, combined with a low cell voltage to avoid the formation of large amounts of gaseous products. However, as already discussed in previous paragraphs, these conditions cannot be replicated in the CO_2RR, since feeding CO_2 leads to its reaction with water to form carbonates and bicarbonates, which in turn lowers the pH.

3.3 A comparison between CuNPs and CuIN@FCX650SE

In this paragraph, we will compare commercial copper nanoparticles (CuNPs) with the newly synthesized catalyst, CuIN@FCX650SE, for carbon monoxide reduction, using a 0.2 M $KHCO_3$ solution as the electrolyte.

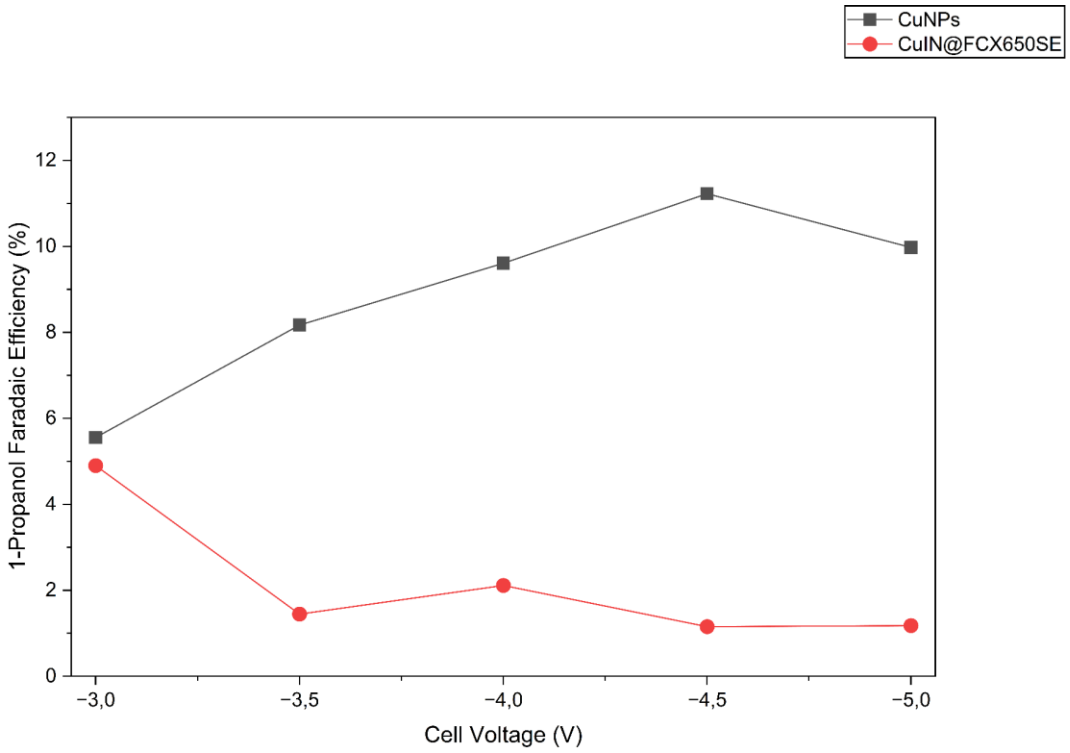
CuNPs
CuIN@FCX650SE
1-Propanol Faradaic Efficiency (%)
0
2
4
6
8
10
12
−3,0
−3,5
−4,0
−4,5
−5,0
Cell Voltage (V)

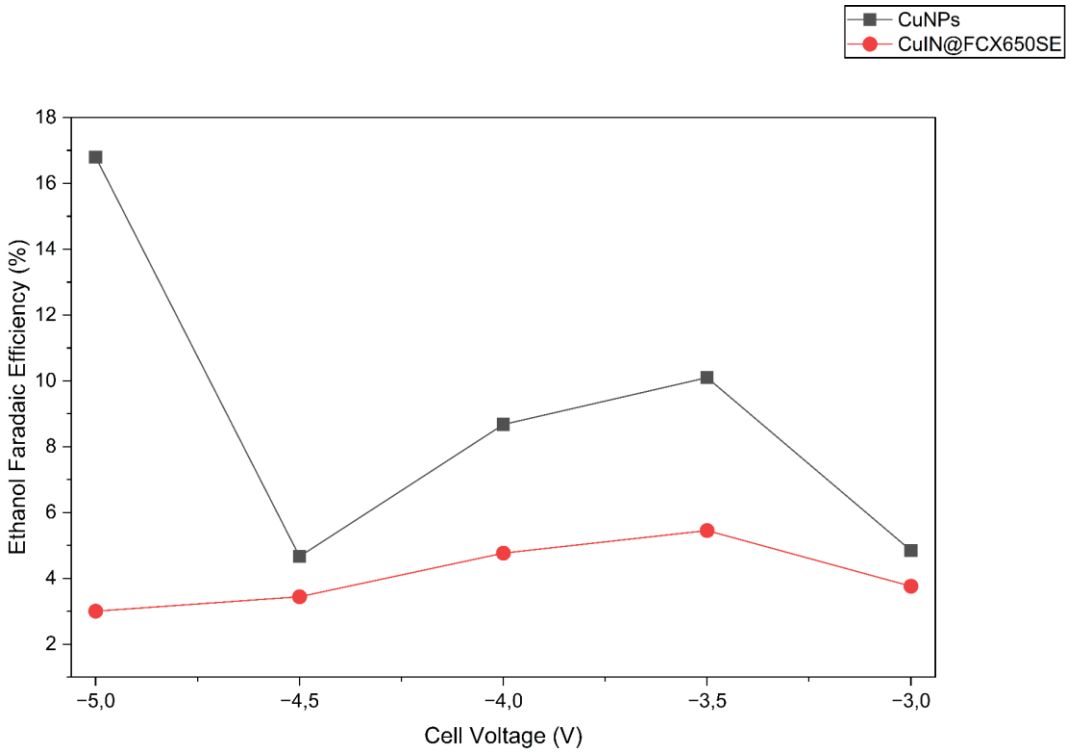
CuNPs
CuIN@FCX650SE
Ethanol Faradaic Efficiency (%)
2
4
6
8
10
12
14
16
18
−5,0
−4,5
−4,0
−3,5
−3,0
Cell Voltage (V)

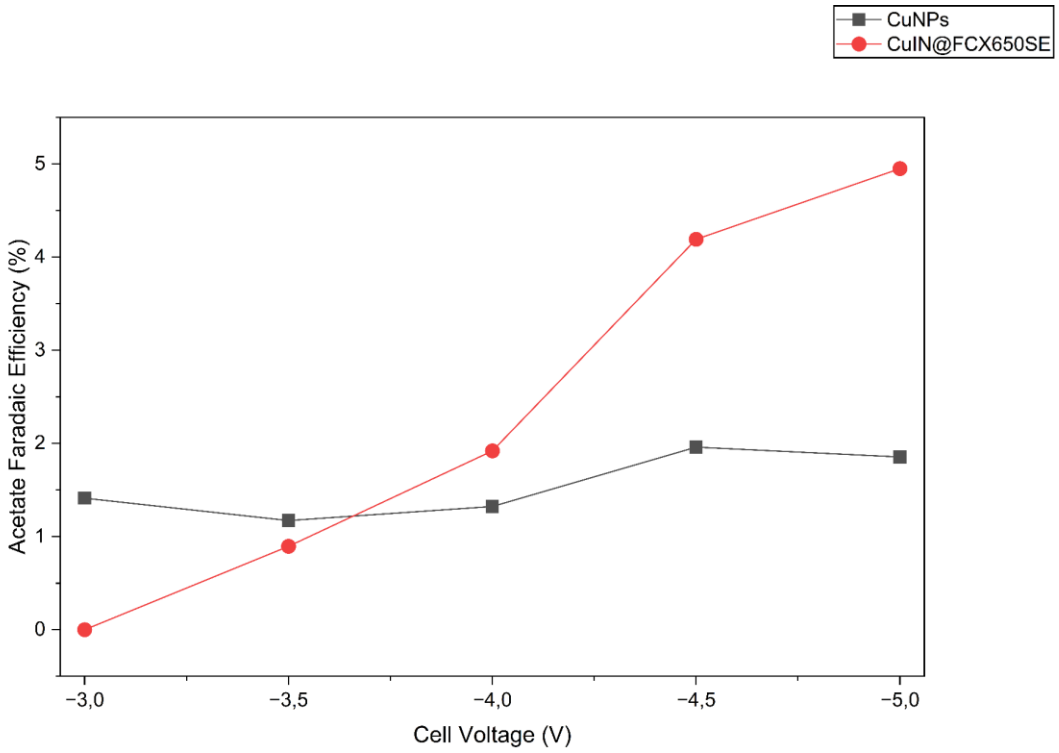

***Figure 31**: Faradaic efficiencies towards Ethanol, 1-Propanol and Acetate for CO reduction at pH 8.5, using CuNPs and CuIN@FCX650SE*

From the graphs in Fig. 31, we can observe the trend of Faradaic efficiencies for the liquid products obtained using the two catalysts. For Ethanol and 1-Propanol, the Faradaic efficiencies achieved with commercial copper nanoparticles are higher compared to CuIN@FCX650SE. However, in the case of Acetate, we obtained promising results: when operating at high cell voltages, from 4 V onwards, the new catalyst delivers higher Faradaic efficiencies than the CuNPs. Nevertheless, these efficiencies remain quite low, as they do not exceed 5%. Still, considering that the new catalyst contains only 13.41 wt% of copper, these results appear encouraging.

3.4 CO_2 reduction results

In this paragraph, we present the results obtained using the four different catalysts for CO_2 reduction. As shown in Fig. 32, the best performances, in terms of total Faradaic efficiency toward liquid products, were achieved with commercial copper nanoparticles, reaching a maximum total Faradaic efficiency of 40.49%. Regarding the other catalysts, the two lowest performances were recorded with CuIN@FCX650SE and Ag@FCX650SE, both reaching a maximum Faradaic efficiency of around 20%. However, by combining these two active sites, using the Cu/Ag@FCX650SE catalyst, the performance improved significantly, and at a voltage of –4 V, we reached a maximum Faradaic efficiency of 31.87%.

In all analyzed samples, the main product obtained was Formate, which is the easiest product to generate from CO_2 in terms of reaction mechanism simplicity. Small amounts of Ethanol and 1-Propanol were also detected, while Acetate, our target product, was not obtained. This once

again highlights the difficulty of producing this compound under the reaction conditions employed for CO_2 reduction.

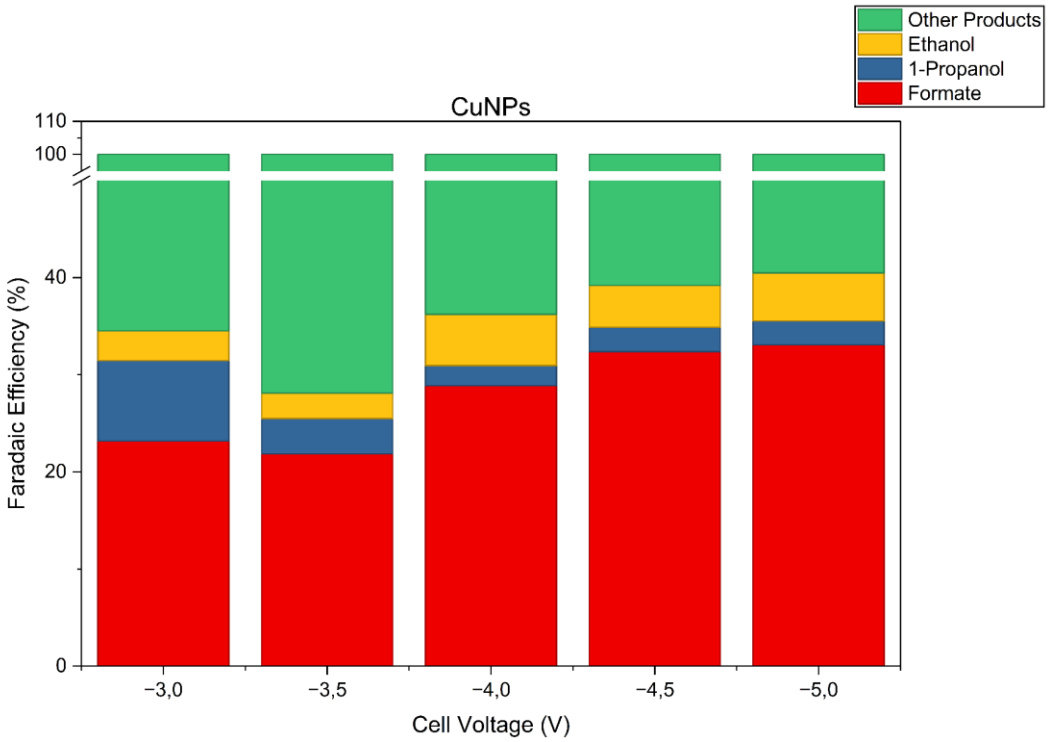

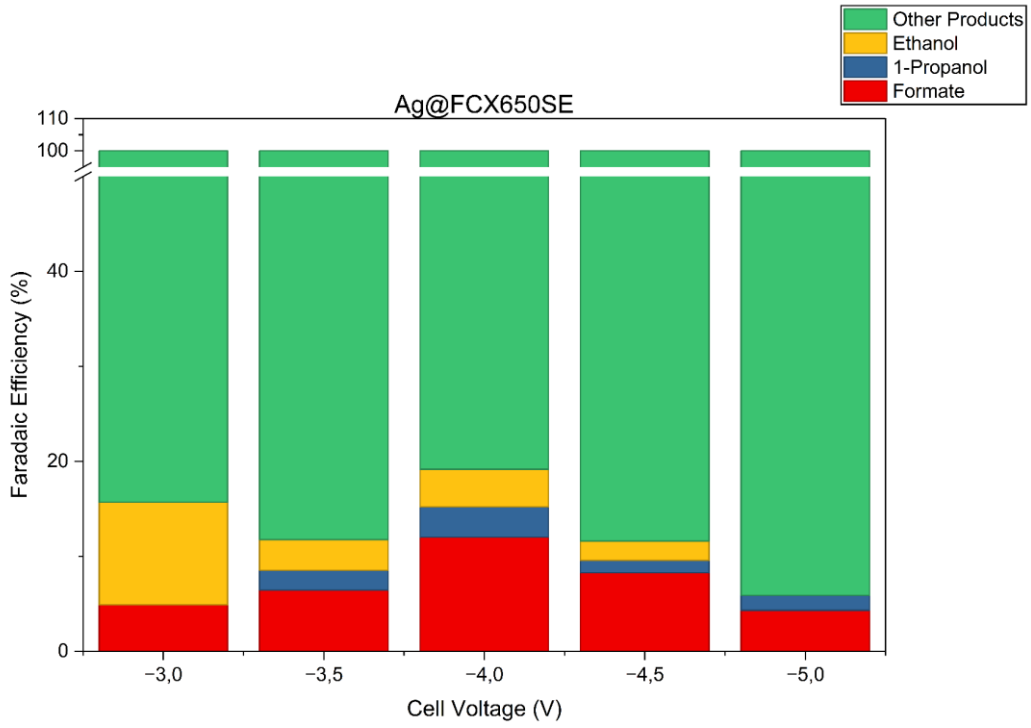

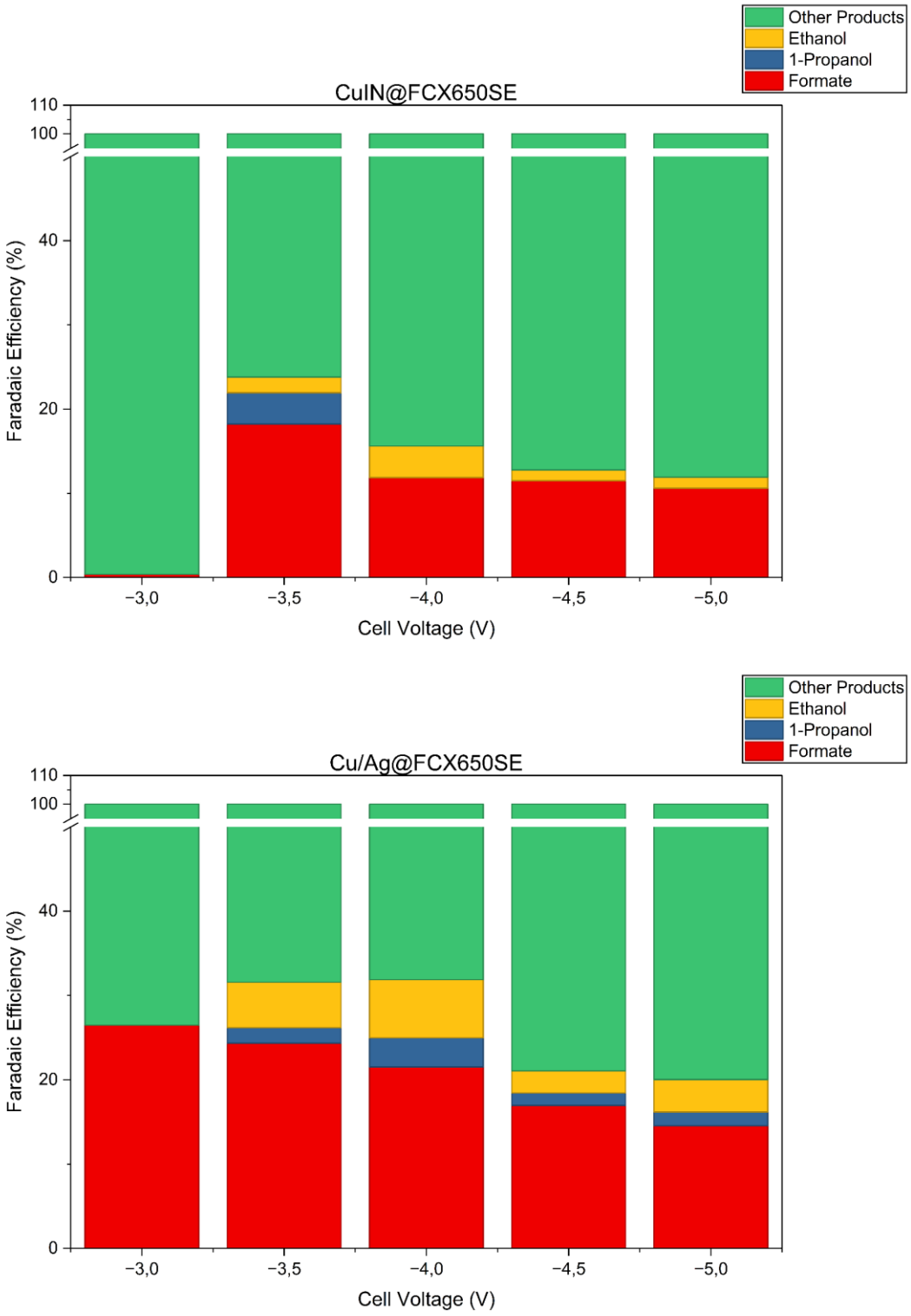

***Figure 32**: Bar chart of the Faradaic Efficiencies of the liquid products for CO2RR, using commercial CuNPs, Ag@FCX650SE, CuIN@FCX650SE, Cu/Ag@FCX650SE*

4. Conclusions and future perspectives

This work set out to explore and enhance copper-based electrocatalysts for the selective production of Acetate. Building on the intrinsic ability of copper to promote C–C coupling in CO_2 reduction, we designed and synthesized new catalytic systems, including CuIN@FCX650SE, comprising copper nanoparticles embedded within a graphitic carbon framework, and a bimetallic hybrid catalyst (Cu/Ag@FCX650SE) obtained by decorating the carbon structure with both copper and silver nanoparticles. Their electrocatalytic behavior was systematically investigated in the CO_2 reduction reaction, while we performed a pH screening of CO reduction reaction using commercial copper nanoparticles.

pH-dependent CORR experiments revealed that high alkalinity (pH 13.5) combined with relatively low cell voltages maximizes Acetate selectivity, reaching a Faradaic efficiency of 23.54% at −3 V. However, these favorable conditions are not directly transferrable to CO_2RR due to unavoidable pH buffering from carbonate/bicarbonate formation. In CO_2RR, commercial copper nanoparticles achieved the highest total Faradaic efficiency toward liquid products (40.49%), while the Cu/Ag hybrid outperformed the individual Cu- or Ag-based catalysts, reaching 31.87% at −4 V. Across all catalysts tested, Formate dominated the liquid product distribution, with only minor Ethanol and 1-Propanol detected, and no Acetate formation under the chosen conditions, highlighting the kinetic and mechanistic challenges in steering CO_2RR pathways toward Acetate in high-rate flow cell environments.

These findings underscore the importance of catalyst composition, active site synergy, and reaction microenvironment in directing selectivity toward targeted oxygenates. Future research could strategically focus on optimizing copper loading in CuIN@FCX650SE, as well as fine-tuning the Cu:Ag ratio in Cu/Ag@FCX650SE, to enhance multi-carbon product yields. Moreover, the synthesis of a true Cu–Ag alloy presents an intriguing opportunity to address mass transport limitations and suppress undesired diffusion of reaction intermediates within the catalyst architecture, potentially unlocking more efficient pathways towards Acetate and other multi-carbon oxygenates. Such advances, coupled with tailored electrolyte engineering, could bring copper-based electrocatalysis closer to industrially relevant Acetate production.

References

[1] Anwar, M. N., et al. (2019). Sources of carbon dioxide and environmental issues. In Inamuddin, A. M., Asiri, A. M., & Lichtfouse, E. (Eds.), *Sustainable Agriculture Reviews* (Vol. 37, pp. 31–70). Springer. https://doi.org/10.1007/978-3-030-29298-0_2

[2] Nunes, L. J. R. (2023). The rising threat of atmospheric CO_2: A review on the causes, impacts, and mitigation strategies. *Environments, 10*(4), 66. https://doi.org/10.3390/environments10040066

[3] International Energy Agency (IEA). (2025). *Global CO_2 emissions from energy combustion and industrial processes and their annual change, 1900–2023*. Retrieved August 12, 2025, from https://www.iea.org/data-and-statistics/charts/global-co2-emissions-from-energy-combustion-and-industrial-processes-and-their-annual-change-1900-2023

[4] Intergovernmental Panel on Climate Change (IPCC). (n.d.). *Sixth assessment report cycle*. Retrieved August 12, 2025, from https://www.ipcc.ch/report/sixth-assessment-report-cycle/

[5] Solomon, S., Plattner, G., Knutti, R., & Friedlingstein, P. (2009). Irreversible climate change due to carbon dioxide emissions. *Proceedings of the National Academy of Sciences of the United States of America, 106*(6), 1704–1709. https://doi.org/10.1073/pnas.0812721106

[6] Acosta-Silva, Y. de J., Torres-Pacheco, I., Matsumoto, Y., et al. (2019). Applications of solar and wind renewable energy in agriculture: A review. *Science Progress, 102*(2), 127–140. https://doi.org/10.1177/0036850419832696

[7] Baena-Moreno, F. M., Rodríguez-Galán, M., Vega, F., Alonso-Fariñas, B., Vilches Arenas, L. F., & Navarrete, B. (2018). Carbon capture and utilization technologies: A literature review and recent advances. *Energy Sources, Part A: Recovery, Utilization, and Environmental Effects, 41*(12), 1403–1433. https://doi.org/10.1080/15567036.2018.1548518

[8] Jhong, H.-R. M., Ma, S., & Kenis, P. J. A. (2013). Electrochemical conversion of CO_2 to useful chemicals: Current status, remaining challenges, and future opportunities. *Current Opinion in Chemical Engineering, 2*(2), 191–199. https://doi.org/10.1016/j.coche.2013.03.005

[9] Appel, A. M., Bercaw, J. E., Bocarsly, A. B., et al. (2013). Chemistry of CO_2 reduction. *Chemical Reviews, 113*(8), 6621–6658. https://doi.org/10.1021/cr300463y

[10] Jouny, M., Luc, W., & Jiao, F. (2018). General techno-economic analysis of CO_2 electrolysis systems. *Industrial & Engineering Chemistry Research, 57*(6), 2165–2177. https://doi.org/10.1021/acs.iecr.7b03514

[11] Hori, Y., Wakebe, H., Tsukamoto, T., & Koga, O. (1994). Electrocatalytic process of CO selectivity in electrochemical reduction of CO_2 at metal electrodes in aqueous media. *Electrochimica Acta, 39*(11–12), 1833–1839. https://doi.org/10.1016/0013-4686(94)85172-7

[12] Whipple, D. T., & Kenis, P. J. A. (2010). Prospects of CO_2 utilization via direct heterogeneous electrochemical reduction. *Journal of Physical Chemistry Letters, 1*(24), 3451–3458. https://doi.org/10.1021/jz1012627

[13] Kortlever, R., Shen, J., Schouten, K. J. P., Calle-Vallejo, F., & Koper, M. T. M. (2015). Catalysts and reaction pathways for the electrochemical reduction of carbon dioxide. *Journal of Physical Chemistry Letters, 6*(20), 4073–4082. https://doi.org/10.1021/acs.jpclett.5b01559

[14] Nitopi, S., Bertheussen, E., Scott, S. B., et al. (2019). Progress and perspectives of electrochemical CO_2 reduction on copper in aqueous electrolyte. *Chemical Reviews, 119*(12), 7610–7672. https://doi.org/10.1021/acs.chemrev.8b00705

[15] Birdja, Y. Y., Pérez-Gallent, E., Figueiredo, M. C., et al. (2019). Advances and challenges in understanding the electrocatalytic conversion of carbon dioxide to fuels. *Nature Energy, 4*, 732–745. https://doi.org/10.1038/s41560-019-0450-y

[16] Hori, Y. (2008). Electrochemical CO_2 reduction on metal electrodes. In Vayenas, C. G., White, R. E., & Gamboa-Aldeco, M. E. (Eds.), *Modern aspects of electrochemistry* (Vol. 42, pp. 89–189). Springer. https://doi.org/10.1007/978-0-387-49489-0_3

[17] Gao, D., Arán-Ais, R. M., Jeon, H. S., & Roldan Cuenya, B. (2019). Rational catalyst and electrolyte design for CO_2 electroreduction towards multicarbon products. *Nature Catalysis, 2*, 198–210. https://doi.org/10.1038/s41929-019-0235-9

[18] Chen, C., Khosrowabadi Kotyk, J. F., & Sheehan, S. W. (2018). Progress toward commercial application of electrochemical carbon dioxide reduction. *Chemical, 4*(12), 2571–2586. https://doi.org/10.1016/j.chempr.2018.08.019

[19] Ross, M. B., De Luna, P., Li, Y., Dinh, C.-T., Kim, D., et al. (2019). Designing materials for electrochemical carbon dioxide recycling. *Nature Catalysis, 2*, 648–658. https://doi.org/10.1038/s41929-019-0306-7

[20] Schreier, M., Yoon, Y., Jackson, M. N., & Surendranath, Y. (2018). Competition between CO_2 reduction and H_2 evolution on a gold electrode under well-defined mass transport conditions. *ACS Energy Letters, 3*(1), 139–143. https://doi.org/10.1021/acsenergylett.7b01054

[21] Zheng, T., Jiang, K., & Wang, H. (2018). Recent advances in electrochemical CO_2-to-CO conversion on heterogeneous catalysts. *Advanced Materials, 30*(48), 1802066. https://doi.org/10.1002/adma.201802066

[22] De Luna, P., Hahn, C., Higgins, D., Jaffer, S. A., Jaramillo, T. F., & Sargent, E. H. (2019). What would it take for renewably powered electrosynthesis to displace petrochemical processes? *Science, 364*(6438), eaav3506. https://doi.org/10.1126/science.aav3506

[23] Dinh, C.-T., Burdyny, T., Kibria, M. G., Seifitokaldani, A., et al. (2018). CO_2 electroreduction to ethylene via hydroxide-mediated copper catalysis at an abrupt interface. *Science, 360*(6390), 783–787. https://doi.org/10.1126/science.aas9100

[24] Kibria, M. G., Dinh, C.-T., Seifitokaldani, A., et al. (2019). Electrochemical CO_2 reduction into chemical feedstocks: From mechanistic electrocatalysis models to system design. *Advanced Materials, 31*(31), 1807166. https://doi.org/10.1002/adma.201807166

[25] Handoko, A. D., Wei, F., Jenndy, Yeo, B. S., & Seh, Z. W. (2018). Understanding heterogeneous electrocatalytic carbon dioxide reduction through operando techniques. *Nature Catalysis, 1*, 922–934. https://doi.org/10.1038/s41929-018-0182-6

[26] Kim, Y., Kim, J., & Lee, H. (2020). Progress in electrochemical reduction of CO_2: Catalyst design, reaction mechanisms, and mass transport. *Chemical Engineering Journal, 390*, 124611. https://doi.org/10.1016/j.cej.2020.124611

[27] Raciti, D., & Wang, C. (2018). Recent advances in CO_2 reduction electrocatalysis on copper. *ACS Energy Letters, 3*(7), 1545–1556. https://doi.org/10.1021/acsenergylett.8b00701

[28] Clark, E. L., & Bell, A. T. (2018). Direct observation of the local reaction environment during the electrochemical reduction of CO_2. *Journal of the American Chemical Society, 140*(22), 7012–7020. https://doi.org/10.1021/jacs.8b04058

[29] Li, C. W., & Kanan, M. W. (2012). CO_2 reduction at low overpotential on Cu electrodes resulting from the reduction of thick Cu_2O films. *Journal of the American Chemical Society, 134*(17), 7231–7234. https://doi.org/10.1021/ja3010978

[30] Ren, D., Deng, Y., Handoko, A. D., Chen, C., Malkhandi, S., & Yeo, B. S. (2015). Selective electrochemical reduction of carbon dioxide to ethylene and ethanol on copper(I) oxide catalysts. *ACS Catalysis, 5*(5), 2814–2821. https://doi.org/10.1021/acscatal.5b00302

[31] Kas, R., Kortlever, R., Milbrat, A., Koper, M. T. M., et al. (2014). Electrochemical CO_2 reduction on Cu_2O-derived copper nanoparticles: Controlling the catalytic selectivity of hydrocarbons. *Physical Chemistry Chemical Physics, 16*(24), 12194–12201. https://doi.org/10.1039/c4cp01520g

[32] Lum, Y., & Ager, J. W. (2018). Stability of residual oxides in oxide-derived copper catalysts for electrochemical CO_2 reduction investigated with 18O labeling. *Angewandte Chemie International Edition, 57*(2), 551–554. https://doi.org/10.1002/anie.201710343

[33] Wang, X., Wang, Z., Garcia de Arquer, F. P., et al. (2019). Efficient electrically powered CO_2-to-ethanol via suppression of deoxygenation. *Nature Energy, 5*, 478–486. https://doi.org/10.1038/s41560-020-0591-1

[34] Gao, D., Zhou, H., Cai, F., Wang, D., Hu, Y., et al. (2017). Size-dependent electrocatalytic reduction of CO_2 over Pd nanoparticles. *Journal of the American Chemical Society, 137*(13), 4288–4291. https://doi.org/10.1021/jacs.5b00406

[35] Lv, W., Zhang, C., Li, Z., et al. (2020). Low-coordination Ag sites in AgCu alloy for selective electrochemical reduction of CO_2 to CO. *Angewandte Chemie International Edition, 59*(2), 679–684. https://doi.org/10.1002/anie.201910578

[36] Jouny, M., Luc, W., & Jiao, F. (2018). General techno-economic analysis of CO_2 electrolysis systems. *Industrial & Engineering Chemistry Research, 57*(6), 2165–2177. https://doi.org/10.1021/acs.iecr.7b03514

[37] Lee, S. H., Lin, J., Lee, J., et al. (2021). Oxide-derived Cu/Ag catalysts for selective electrochemical reduction of CO_2 to multicarbon products. *ACS Catalysis, 11*(1), 776–784. https://doi.org/10.1021/acscatal.0c04315

[38] Kim, D., Resasco, J., Yu, Y., Asiri, A. M., & Yang, P. (2014). Synergistic geometric and electronic effects for electrochemical reduction of carbon dioxide using gold–copper bimetallic nanoparticles. *Nature Communications, 5*, 4948. https://doi.org/10.1038/ncomms5948

[39] Chen, Y., Li, C. W., & Kanan, M. W. (2012). Aqueous CO_2 reduction at very low overpotential on oxide-derived Au nanoparticles. *Journal of the American Chemical Society, 134*(49), 19969–19972. https://doi.org/10.1021/ja309317u

[40] Zhao, K., Liu, Y., Quan, X., Chen, S., Yu, H., & Zhao, H. (2016). Selective electroreduction of carbon dioxide to formate on a Cu(100) surface in ionic liquid/water system. *ACS Catalysis, 6*(8), 5393–5398. https://doi.org/10.1021/acscatal.6b00987

[41] Qiao, J., Liu, Y., Hong, F., & Zhang, J. (2014). A review of catalysts for the electroreduction of carbon dioxide to produce low-carbon fuels. *Chemical Society Reviews, 43*(2), 631–675. https://doi.org/10.1039/c3cs60323g

[42] Wang, G., Chen, J., Ding, Y., Cai, P., Yi, J., Li, Y., & Li, Y. (2020). Engineering the local reaction environment of bimetallic electrocatalysts for CO_2 reduction. *Journal of Materials Chemistry A, 8*(19), 9650–9661. https://doi.org/10.1039/d0ta02006c

[43] Higgins, D., Hahn, C., Xiang, C., Jaramillo, T. F., & Weber, A. Z. (2019). Gas-diffusion electrodes for carbon dioxide reduction: A new paradigm. *ACS Energy Letters, 4*(1), 317–324. https://doi.org/10.1021/acsenergylett.8b02035

[44] Li, J., Che, F., Pang, Y., et al. (2018). Copper alloy surfaces with high selectivity for electrochemical CO_2 reduction to ethylene. *Nature Catalysis, 1*, 592–600. https://doi.org/10.1038/s41929-018-0100-6

Ringraziamenti

Ai miei genitori, per il loro supporto costante nei momenti difficili e per la loro presenza in quelli importanti. Se questo percorso è andato nel migliore dei modi, il merito è soprattutto vostro.

A Nino, Ludovico, Peppe, Alessandro, Pietro e a tutti i ragazzi conosciuti in questi quattro anni a Torino: non avrei potuto desiderare una compagnia migliore per affrontare una fase così importante della mia vita.

Ai ragazzi di Montagano, che resteranno sempre il mio porto sicuro e il posto che continuerò a chiamare casa.

Ad Alfonso e Antonio, grazie per aver condiviso con me questi anni sotto lo stesso tetto, per la serenità quotidiana e per i momenti leggeri che hanno reso speciale la nostra convivenza.

A Yu-Han, Giovanni, Alessio, Camille, Loki, Daniele, Chris e a tutti gli amici conosciuti in California: avete reso quell'esperienza indimenticabile, e porterò con me ogni ricordo per sempre.